DArk Sector Experiments at LCLS-II

Letter of Intent

Authors: Tony Beukers (SLAC), Alan Fry (SLAC), Carsten Hast (SLAC), Thomas W. Markiewicz (SLAC), Timothy K. Nelson (SLAC), Yuri M. Nosochkov (SLAC), Nan Phinney (SLAC), Tor O. Raubenheimer (SLAC), Philip C. Schuster (SLAC), Natalia Toro (SLAC), on behalf of the DASEL Design Group

9/12/2016

1 Executive Summary

Identifying the particle content of dark matter is one of the most important challenges facing fundamental physics today; the answer will shape the field for many decades to come. Experiments aiming to produce and study dark matter using particle accelerators, in much the same way that key elements of the Standard Model were discovered, are an essential component of the search for dark matter. In particular, for an important class of light dark matter scenarios, electron fixed-target experiments are uniquely robust and have unparalleled sensitivity.

To that end, the construction of LCLS-II for SLAC's photon science program presents a unique, timely, and cost-effective opportunity to enable and host high-impact dark matter and dark force experiments. We summarize here the initial concept behind DArk Sector Experiments at LCLS-II (DASEL), which will deliver a low-current, continuous electron beam to End Station A (ESA) by filling unused buckets from the LCLS-II linac and building a new kicker and transfer beamline to divert them into the existing ESA beamline. Importantly, DASEL extracts beam downstream of the LCLS-II x-ray lines and, therefore, does not affect LCLS-II operations.

DASEL's multi-GeV energy, high beam repetition rate and capability to host year-scale particle physics experiments offer a unique combination of advantages that make possible a wide range of world-class experiments. The first phase of DASEL supports sub-nA beam currents at ESA for the Light Dark Matter eXperiment (LDMX), currently under development. LDMX is designed to decisively test thermal dark matter in the MeV-GeV mass range, a goal that no other existing or planned experiment can achieve.

Testing thermal dark matter is a major priority for particle physics and cosmology. Hosting LDMX would place SLAC at the top of a highly competitive international effort to explore the physics of light dark matter. Two LDMX science runs at DASEL are projected to take place during the 2021-2025 timeframe. Modest upgrades to the DASEL gun-laser systems and beamline diagnostics would enable operation at currents of up to 2 μA, supporting complementary experiments using high-statistics electron-positron pair production to search for GeV-scale force carriers in currently unexplored parameter space.

The total cost for the DASEL project is estimated to be under ten million dollars, including a contingency appropriate for the present design maturity of each subsystem. The timeline for design and early procurements is tight because the LCLS schedule precludes major installation in the Beam Switchyard (BSY) after March of 2019. It is therefore essential to procure beamline hardware and finalize the design of beamline controls during FY 2018 in order to install this beamline during the first half of FY 2019, while regular access to the BSY is still possible.

Design efforts thus far have focused on a conceptual design for the purposes of: (a) feasibility demonstration; (b) obtaining a credible cost estimate for DASEL, and (c) assuring that DASEL installation and operations do not interfere with LCLS-II. This design effort and the resulting cost and schedule are summarized in this Letter of Intent.

2 Physics Motivation

The identity of dark matter is one the most pressing open questions in fundamental physics today. Searching for dark matter is one the major areas prioritized by the particle physics community in the P5 report and by the Laboratory in its strategic plan.

Among the best-motivated possibilities is that dark matter might be composed of particles that were produced during an era of thermodynamic equilibrium in the early universe and survived to the present day as a "thermal relic". Within this framework, the possibility that dark matter particles have mass similar to familiar matter, in the MeV-GeV range, is compelling but largely unexplored. This simple scenario is realized by a "dark sector" containing the dark matter particle, a new force carrier of comparable mass, and possibly other accompanying particles. Although these particles couple weakly to familiar matter, the observed dark matter abundance implies a lower bound on the coupling in simple models, which is accessible in high-sensitivity, fixed-target experiments.

This possibility has spurred a broad international program of experiments searching for dark forces and light dark matter, including dedicated experiments at Jefferson Lab (APEX [1], HPS [2], DarkLight [3], BDX [4]), Mainz [5], INFN Frascati (PADME [6]), and CERN (P348/NA-64 [7]). The search for dark sectors was one of five focal areas for the 2013 Snowmass process [8]; has twice been the subject of APS mini-symposia [9]; and was the subject of recent dedicated international meetings at Frascati [10], Brookhaven [11], and Genova [12], and, most recently, of the SLAC Dark Sectors Workshop [13].

Multi-GeV continuous electron beams are particularly well suited to these experiments. The APEX and HPS experiments at Jefferson Lab's Continuous Electron Beam Accelerator Facility (CEBAF), both of which have SLAC researchers in leadership roles, are flagship efforts involving more than 100 scientists at 35 institutions in 7 countries. The next generation of experiments does not require the beam polarization or precisely tunable energy of CEBAF, but requires sustained low beam currents for which CEBAF was not designed, as well as extensive run times and real physics priority. These experiments are very unlikely to be implemented at CEBAF given the facility's 10-year backlog of experiments and the priority of nuclear physics at JLab.

Two experimental proposals are being developed in tandem with the accelerator design summarized here and serve as benchmarks to inform DASEL beam requirements. LDMX employs a "missing momentum" approach [14] searching for electroproduction of light dark matter that calls for a diffuse beam at very low current (5-300 pA scale) impinging on a target with tracking and a high-granularity calorimeter directly in the beamline, so that the trajectories of individual beam electrons and their byproducts through the detector can be reconstructed in detail. This approach has unique potential to explore interaction strengths at the lower bound consistent with thermal dark matter (see Fig. 1). It would also decisively test the hypothesis that dark matter annihilates into familiar matter in much of the sub-GeV mass range [15]. Section 2.3 provides a summary of the LDMX concept. A second concept, SuperHPS, [16] would extend HPS sensitivity by configuring HPS-like detectors downstream of an analyzing magnet to

increase acceptance, improve mass resolution, and support higher beam currents in the μA range.

2.1 DASEL Capabilities and Experiments

The DASEL beamline, parasitic to LCLS-II, delivers multi-GeV electrons at up-to-186 MHz repetition rate, with currents ranging from 1 pA to 1 μA. This performance offers SLAC the unique opportunity to host the next generation of cutting-edge dark matter and dark force experiments. We refer to the new beamline and facility collectively as DArk Sector Experiments at LCLS-II (DASEL). Among the most considerable strengths of DASEL is its ability to support experiments capable of searching for both dark matter and any new forces mediating dark matter interactions. The flagship effort, scheduled to begin as early as 2020, focuses on directly observing dark matter production in electron-nuclear fixed-target collisions with sufficient sensitivity to providing a decisive test of thermal dark matter in much of the sub-GeV mass range. Future experiments could expand sensitivity to dark photons after the completion of LDMX. Below, we summarize the flagship Light Dark Matter eXperiment (LDMX) effort and comment on a new force experiment, Super-HPS. A more detailed design report for LDMX will be published by the end of 2017.

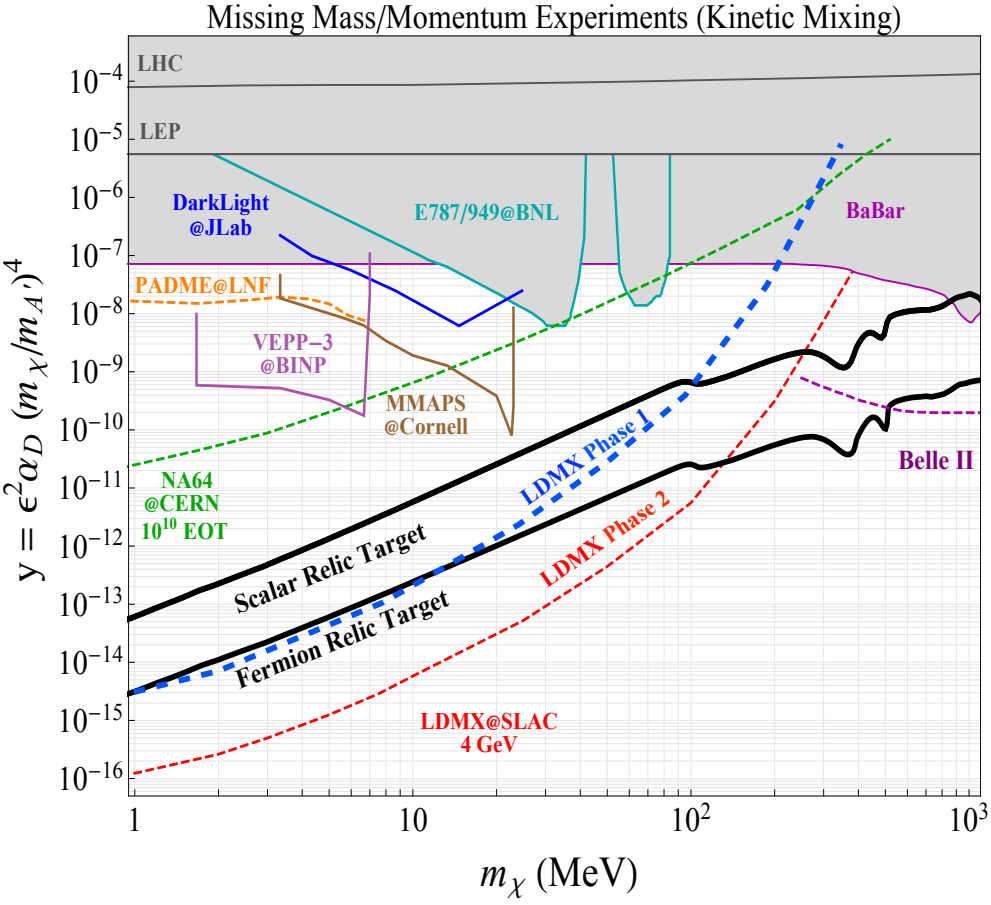

Figure 1. Yield-limited dark matter sensitivity of LDMX at DASEL (blue-dashed for Phase 1 and red-dashed for Phase 2) vs. existing constraints on dark matter production at

accelerators (shaded) and projected sensitivities for other proposed experiments. The y-axis is a dimensionless interaction strength, while the black line is the minimum interaction strength consistent with thermal relic dark matter. Assumptions for missing momentum yields are as in Scenario III of [13] but shown for a 4 GeV beam.

2.2 Experiment Installation and Operations Timeline

This section outlines a possible timeframe for installing and operating the LDMX and SuperHPS experiments at DASEL.

The LDMX collaboration aims to have a substantial portion of the full detector ready to be installed starting in early 2020 for an engineering run, followed by a first science run with the full detector in 2021. The detector design described below is appropriate for the initial science run. The goal is a zero-background search for dark matter production with $4x10^{14}$ electrons on target, leading to level of sensitivity indicated by the dashed blue line shown in Fig. 1. This first-phase detector is designed for an incident electron rate of about 40 MHz, and is hence well matched to the 46.5 MHz frequency of the LCLS-II laser oscillator, with an average of one electron per pulse. With the anticipated DASEL duty cycle of 55% and assuming 90% efficiency of beam delivery from the linac, the science run would take at least eight months. In late 2022, the LDMX collaboration would upgrade to a detector that can maintain low background with 30 times higher electron flux. The upgraded detector would be ready for a similar-length run starting early in CY 2023, with a level of sensitivity indicated by the dashed red line shown in Fig. 1. It is not yet clear whether the second phase of LDMX could continue to run with a 46.5 MHz beam, with 30 electrons per bunch, or would require a DASEL laser upgrade (requiring a new IR laser for DASEL, separate from the LCLS-II gun laser, with an oscillator frequency of 186 MHz to match the full gun RF frequency).

This schedule allows for possible commissioning and data-taking by the Super-HPS experiment in 2024-25 and an end to End Station A operations by 2026, when LCLS-II may expand with new undulator beamlines in End Station A. This plan is only indicative and subject to significant uncertainty.

2.3 Example of a High-Impact DASEL Experiment: LDMX

The LDMX experiment proposes a high-statistics search for low-mass dark matter at the DASEL beamline using the missing momentum technique, which scatters incoming electrons in a tungsten target to produce dark matter via “dark bremsstrahlung.” Dark matter production events are identified by individually tagging incoming beam-energy electrons, unambiguously associating them with low energy, moderate transverse-momentum recoils and establishing the absence of a forward-going photon. The primary backgrounds are generated by hard bremsstrahlung in the target, followed by photonuclear reactions occurring in either the target or the forward calorimeter. Therefore, the experiment requires a high-speed, granular calorimeter with MIP sensitivity to identify the products of photo-nuclear reactions, in addition to the low-mass tracking that provides high-purity tagging for incoming electrons and clean, efficient reconstruction of recoils. The LDMX concept proposes to meet these challenges by

leveraging technology under development for the HL-LHC and experience from the HPS experiment.

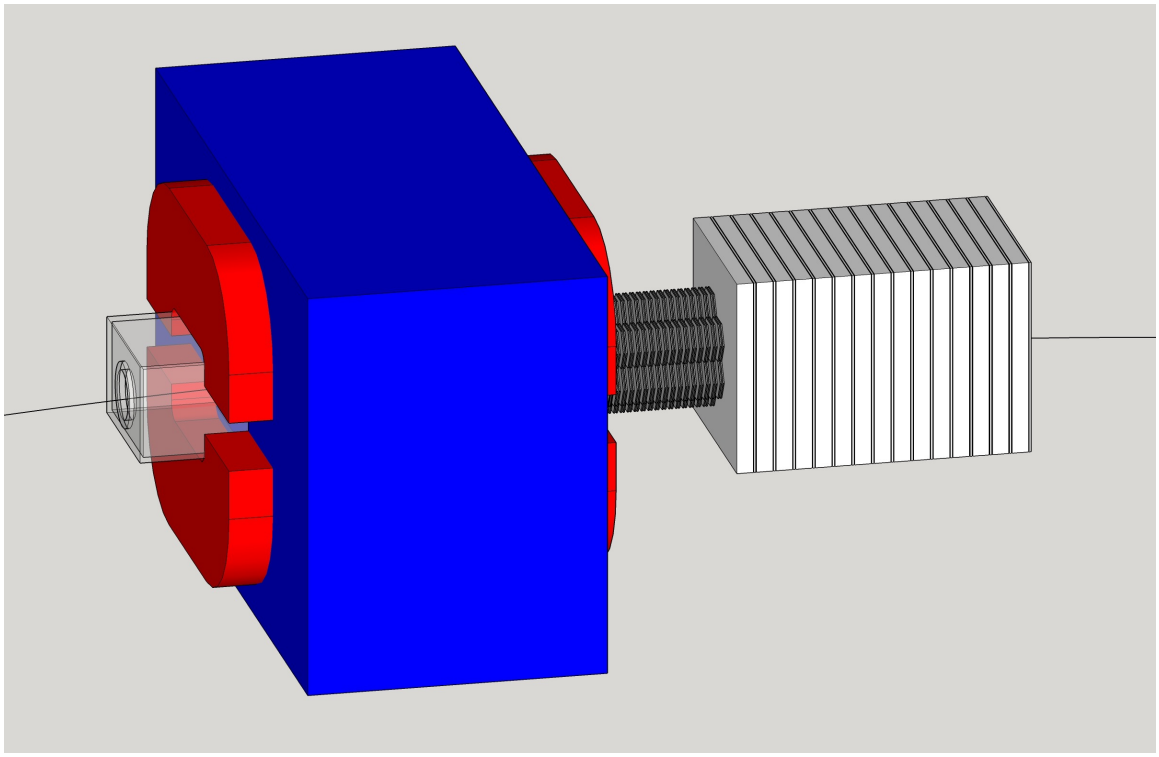

Figure 2. An overview of the LDMX detector showing the vacuum chamber for the trackers inside the spectrometer magnet upstream of the hexagonal modules of the HGC ECal and the larger square modules of the HCal. The DASEL beamline connects to the 6" flange on the upstream end of the vacuum chamber at left.

The two tracking systems required for LDMX, the tagging tracker and the recoil tracker, have similar but distinct requirements. The tagging tracker must tag incoming beam-energy electrons with high purity to eliminate the possibility that a fake beam-energy track could be associated with a recoil. This is accomplished with a highly redundant set of silicon tracking planes immersed in a large, uniform magnetic field. The recoil tracker must provide efficient identification of recoiling electrons over a wide range in momentum and production angle. It uses a set of tracking planes similar to those in the tagging tracker, but in the fringe field of the magnet. While the tagging tracker is large longitudinally and small laterally to purify the sample of incident electrons, the recoil tracker is the opposite, allowing for the tracking of wide-angle recoils while minimizing the distance between the target and the calorimeter, and therefore the size of the calorimeter required for good angular coverage of wide-angle bremsstrahlung. In order to minimize production of secondaries in the trackers, low-mass silicon is required and the trackers are placed inside of the beam vacuum. Maximizing the high-statistics potential of the experiment calls for the finest spatial and temporal resolutions and lowest noise in both trackers. In particular, given the 21 ns bunch timing of the DASEL beamline, time resolution on the order of 1 ns is desirable.

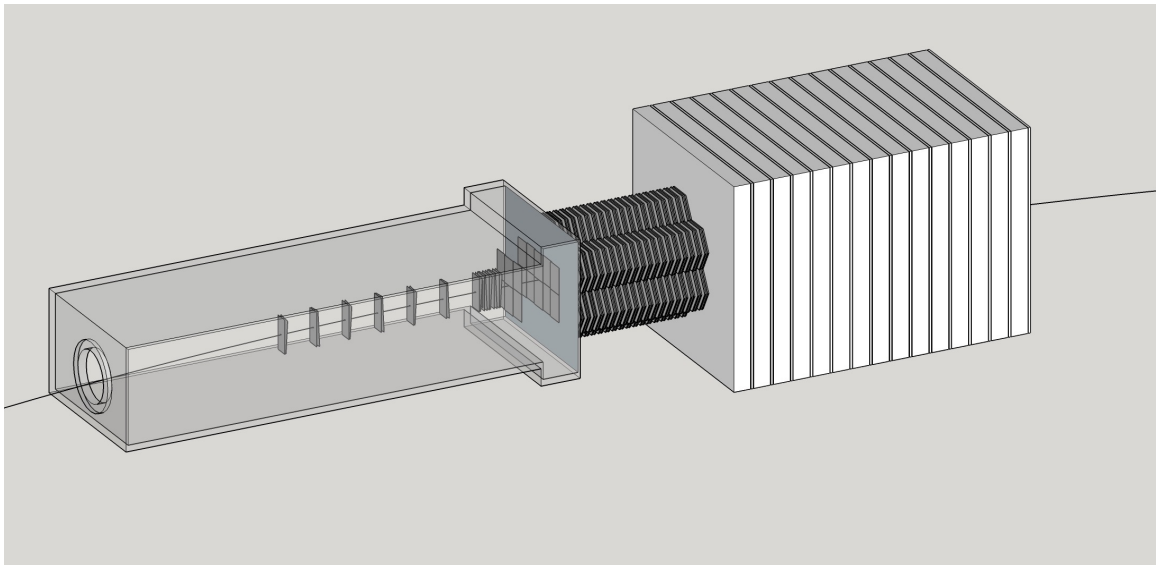

Figure 3. The key components of LDMX with the magnet removed. The trajectory of an incident 4 GeV electron entering the apparatus from the left is shown.

The tagging tracker has seven tracking planes spaced every 10 cm upstream of the target. Each station is a module similar to those for the HPS experiment, which uses single-sided microstrip sensors read out by CMS APV25 chips to achieve excellent spatial and temporal resolution. In each module, sensors are paired into double-sided modules, with 100 mrad stereo for 6 (60) micron resolution in the bend (non-bend) plane; they are tensioned with no support structure in the tracking volume to yield a material budget of 0.6% X_0 per 3D measurement. Multi-peak readout of the APV25 chip results in 2 ns time resolution and the ability to resolve two hits in the same strip separated by at least 50 ns. The target is placed at the edge of the fringe field, only 7.5 mm downstream of the last tagging plane to allow for the best impact parameter resolution. The first four layers of the recoil tracker are identical to the modules for the tagging tracker, placed every 15 mm, with the first layer 7.5 mm downstream of the target. These layers provide redundant 3D tracking to determine the impact location, as well as to precisely measure the initial angle of the recoil. The curvature of high-momentum tracks is poorly measured by such closely spaced planes; therefore, two layers of single-sided microstrips are placed in the space before the front face of the ECal, 90 mm and 180 mm downstream of the target, in order to improve the measurement of this curvature. These layers are much larger in order to maximize acceptance and increase the number of hits, especially for low-momentum tracks, where good track purity is difficult to achieve.

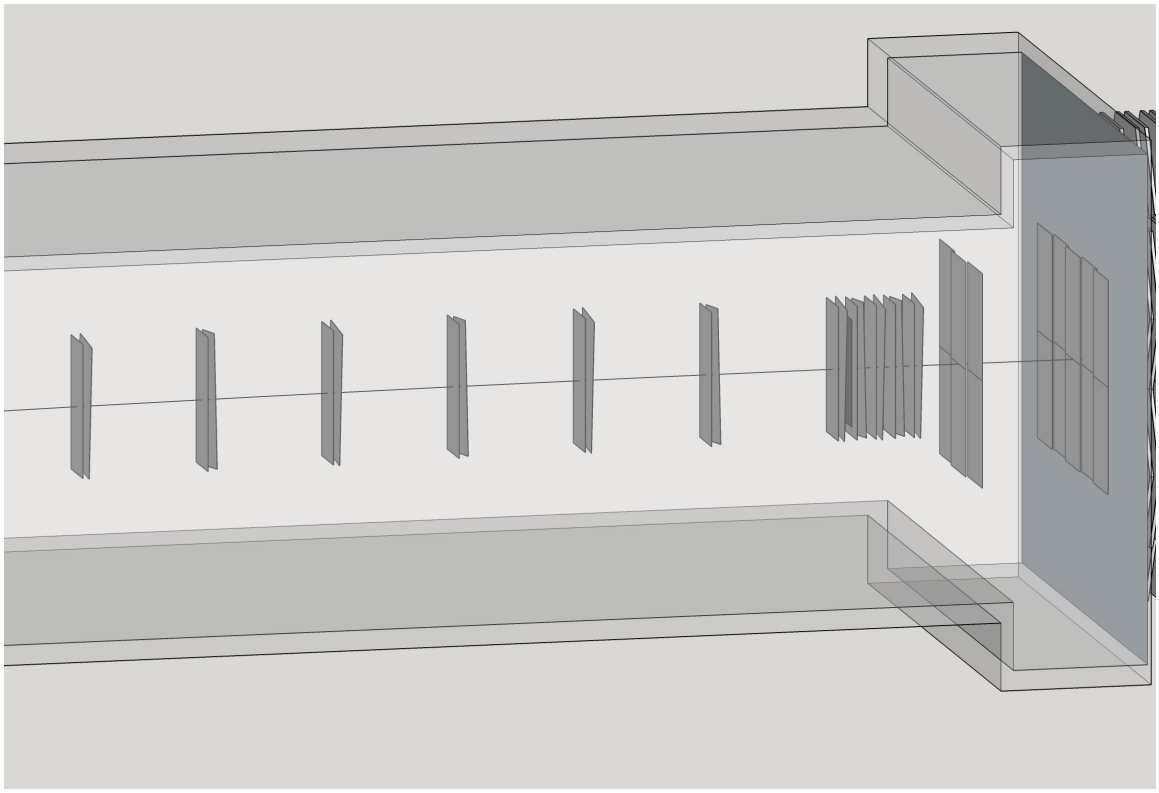

Figure 4. A closeup view of the trackers. The seven stereo pairs of silicon sensors on the left show the tagging tracker (light grey), followed by the 10% X_0 tungsten target (dark grey), with the six-layer recoil tracker shown at right (light grey). The tracker uses only two module designs: one for the tagging tracker and the first four layers of the recoil tracker, and another one for the last two layers of the recoil tracker, which are single-sided and have larger acceptance.

The entire tracker sits inside a stainless steel vacuum chamber with 0.5” walls, with data-acquisition and power distributions boards similar to the HPS Front End Boards (FEBs) and sitting on the upstream positron side in a low radiation environment. Vacuum feedthroughs for power and data are located at the upstream end and copy the HPS designs. Like HPS, the detector and FEBs require cooling but with far less irradiation of the silicon; water is anticipated to be sufficient for both detector and FEB cooling. A thin titanium vacuum window at the downstream end of the vacuum chamber minimizes interactions in dead material in front of the ECal.

The calorimeter design for LDMX is based on the technology of the High Granularity Calorimeter (HGC) of the CMS experiment, now under development for the HL-LHC program at CERN. The electromagnetic part of the HGC is a silicon/tungsten calorimeter with 42 sampling layers that use hexagonal silicon sensors. The sensors are sized to use as much of a 6” or 8” wafer as possible. Prototype sensors on 6” wafers have already been received from Hamamatsu Photonics (HPK) and 8” sensors will be produced by several vendors this year. The CMS/CERN program also includes the development of a front-end ASIC with fast timing capability, and all other front-end and downstream electronics required for triggering and data acquisition. The CMS HGC will be developed in stages, with a fully functional pre-series system scheduled to be ready

by 2020 and a 10% pre-production of modules completed by mid-2021. The total silicon area required for the CMS HGC is 589 m^2, corresponding to ~24,000 modules with sensors from 8" wafers. By comparison, the LDMX experiment will need roughly 200-250 modules. The CMS pre-series system will include a prototype wedge with final components at 3-5% scale for test beam studies. The most important parts of the readout chain should be appropriate for LDMX without modification. Other aspects, such as services, are significantly simpler to handle in the fixed-target configuration of LDMX compared to the collider detector configuration of CMS, so LDMX may make more-rapid progress than CMS. Triggering and downstream readout would be customized for LDMX.

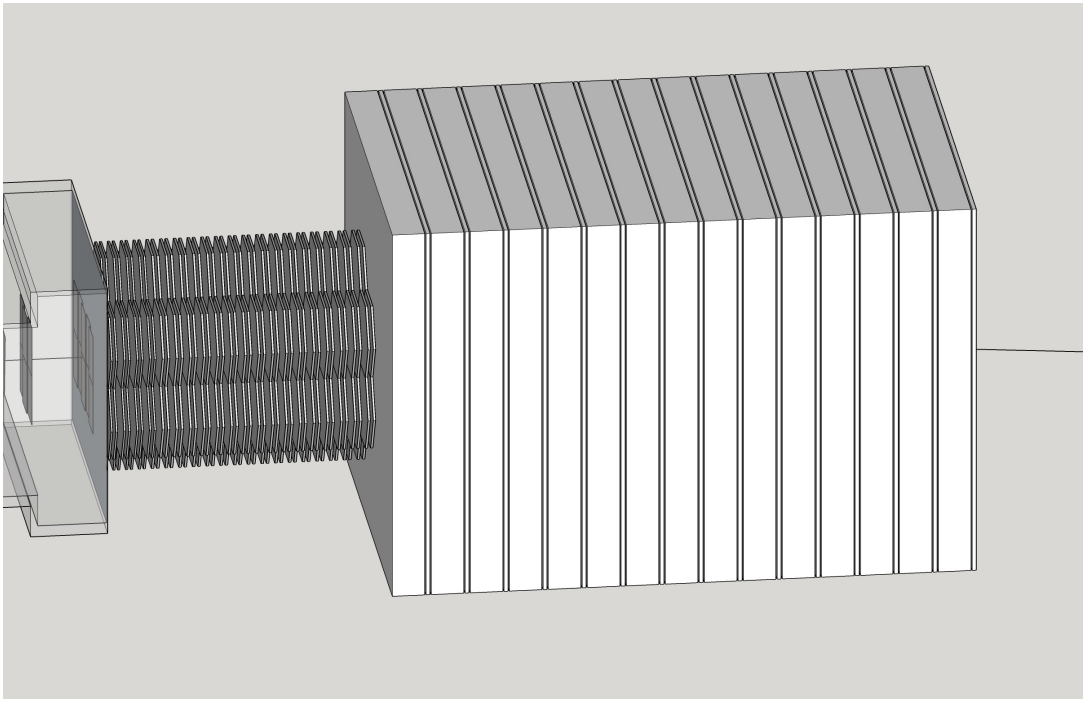

Figure 5. A closeup of the 42-layer HGC ECal (10X 0.8 X_0 + 32X 1 X_0 tungsten) and the 15-layer (5 l) scintillator-based HCal.

The HGC technology is an ideal candidate for the LDMX experiment. Several members of the HGC project are now involved in transferring this technology as it is refined. The main advantages of this technology for LDMX are the high efficiency, granularity, fast response, and radiation tolerance of HGC silicon sensors. The HGC EM calorimeter is expected to have about 30 layers of silicon, each with nearly 100% efficiency for detecting a MIP in their active regions, which make up around > 95% of total surface area. For spatial resolution, an EM shower is 68% contained to a lateral size of the order of a few millimeters in the first layers of the calorimeter and does not reach the Moliere radius (of order 2.8 cm) until more than halfway through the EM calorimeter. The localization of showers from individual incident particles is important for LDMX in discriminating a number of backgrounds and in disentangling overlaps of incident photons and electrons. It is expected that the fast response of silicon, together with extremely low-jitter front end electronics, could allow fast timing resolution on the order

of 50 to 100 ps per channel for pads receiving significant energy deposition. The potential for such fast timing resolution is important to the LDMX program in its later stages, when it will be necessary to have up to 10^9 electrons/second on target in order to achieve sensitivity to the region of lowest couplings in the parameter space that we need to cover. Finally, the well-understood high radiation tolerance of silicon is also important in the long run.

The international project leaders for CMS HGC have indicated their openness to support this collaboration. Taking the lead at the current stage of conceptual design studies are UC Santa Barbara (UCSB) and the University of Minnesota (UMN). Both institutions have a significant involvement with this project in leadership roles. The synergy between the HGC and LDMX is likely to result in mutual benefits, and also serves to avoid the cost of a second major calorimeter development program.

Another important consideration for LDMX is to extend the calorimeter to veto the neutral hadrons produced in photo-nuclear reactions. Considering that photo-nuclear reactions are rare and that conventional electromagnetic showers are fully contained in the HGC, the rates and radiation doses expected in the hadronic calorimeter are much lower than those in the HGC. A scintillator-based sampling calorimeter is a natural solution in this situation. The goal of the hadronic veto system is to identify neutral hadrons in the energy range from above approximately 100 MeV to several GeV with high efficiency. This requires a hadronic calorimeter with a depth of at least five nuclear interaction lengths in order to fully contain the most energetic neutrons with greater than 99% probability. At the same time, in order to detect lower energy neutrons, absorbing layers cannot be so thick that neutrons of hundreds of MeV are captured by them. Therefore, a steel-scintillator (polystyrene) calorimeter of approximately 15 layers and total thickness of five nuclear interaction lengths is proposed. Transverse granularity of the system is not required due to the lower rates expected in the hadronic system and in order to maintain high efficiency for neutral hadron detection.

Fast readout for the hadronic calorimeter system is also required. Readout is based on the CMS Phase 1 upgrade HCAL system, which is capable of fast readout at 40 MHz as is needed for the DASEL beam structure. Scintillating light is read out by wavelength-shifting fibers with silicon photomultipliers (SiPMs). SiPM technology is chosen due to its high gain and low noise capabilities. In addition, readout modules of 48/64 channels and charge-integration electronics designed for the CMS detector can be re-purposed for the LDMX experiment with minimal changes. The timescale for commissioning the readout electronics for CMS is 2017-18, in line with the LDMX timeline.

3 DASEL Design Overview

DASEL uses the SLAC LCLS-II linac to provide a low-current, continuous beam to the experiments. The LCLS-II is an x-ray free electron laser based on a 4.0 GeV superconducting linac. The linac operates with an RF frequency of 1.3 GHz and is fed from an RF gun operating at up to 186 MHz, the seventh sub-harmonic of the RF linac. The baseline LCLS-II design has a maximum bunch rate of 929 kHz, corresponding to a bunch separation of 1,400 1.3-GHz RF buckets. Two high-speed kickers can deflect FEL

bunches towards either the soft x-ray (SXR) or hard x-ray (HXR) undulators; unused beam travels to a high-power dump in the Beam Switch Yard (BSY). The initial phase of the LCLS-II linac accelerates up to 250 kW (nominally 62 μA at 4.0 GeV) of electrons to the BSY; an upgrade path is available to increase the beam current to 300 μA and the power to 1,200 kW by upgrading the 1.3 GHz RF system.

DASEL takes advantage of the "empty" buckets between the LCLS-II bunches. These buckets are populated with very low "dark" current from the LCLS-II RF gun at 186 MHz (5.4 ns spacing) or seeded by a 46-MHz laser oscillator to produce a well-defined, low-current beam with 21.6 ns bunch spacing. The current for DASEL is a small fraction of the nominal LCLS-II current of 62 μA. The DASEL "dark" bunches are diverted to the DASEL beamline and sent to End Station A (ESA) with a third (new) kicker. A 250-meter long beamline takes the dark current from the DASEL kicker/septum system to connect to the existing ESA beamline, where the beam is further collimated. The secondary gun laser and a spoiler/collimation system control the charge delivered to DASEL. This concept is parasitic to LCLS-II operation, since the DASEL beam is low-current (<1μA compared to 62 μA nominal LCLS-II current) and is deflected downstream of the kickers that direct the primary beams to the undulators.

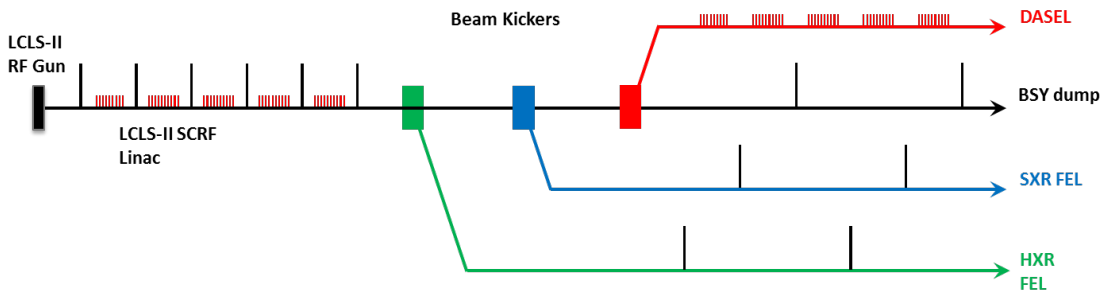

Figure 6. Schematic of DASEL beam from LCLS-II superconducting linac. The DASEL beamline would direct unused beam to End Station A downstream of the extractions to the LCLS-II undulators.

The DASEL concept is illustrated in Figure 6. It would modify the LCLS-II with three additions:

- A low-power photo-cathode laser operating at 46 MHz to supplement the natural dark current being emitted at 186 MHz;
- A long-pulse kicker and septum onto the beamline headed to the BSY dump;
- A 250-meter long beamline extending from Sector 30 through the BSY to connect with the End Station A beamline.

In addition, the ESA spoiler, collimator, and stopper systems are used. Further modifications may be required in the ESA beamline to provide the focusing and possibly rastering desired for the experiment.

The control system for DASEL uses standard LCLS-II modules and software wherever possible. In particular, the timing system is the standard LCLS-II timing system and the safety systems are integrated with the LCLS-II safety systems. Existing infrastructure

and facilities are used both at the laser and in the DASEL beamline. No additional electrical distribution, water, or other facilities are required.

Described in the following sections are: the DASEL overall parameters, Section 3.1; the new laser system, Section 3.2; the new BSY beamline, Section 3.3; the new kicker and septum, Section 3.4; the ESA facility, spoiler/collimator system in the A line, and modifications for DASEL to the end station, Section 3.5; diagnostics and tuning systems, Section 3.6; and radiation protection issues, Section 3.7.

3.1 DASEL Systems Parameters

The parameters of the DASEL system are listed in Table 1. Three categories of parameters are listed: beam at the experiment, beam in the End Station A beamline with the spoiler/collimator system, and beam in the LCLS-II accelerator. Parameters are listed for both the LDMX experiment and a possible subsequent Super-HPS type experiment. The primary beamline is designed to meet the LDMX requirements with the capability of being upgraded to support a future higher-current Super-HPS type experiment.

The DASEL kicker extracts roughly 600 ns of bunches between the LCLS-II primary bunches spaced by 1.1 μs, as illustrated in Figure 7. At the LDMX experiment, the desired electron current ranges between 100 fA and 125 pA, corresponding to from 1 to approximately 500 electrons per μs, or a maximum of 0.5 Watts of electron beam power at 4 GeV.

The buckets to be extracted by the DASEL kicker are filled at the RF gun. The LCLS-II RF gun specification [17] is that dark current is less than 400 nA at 100 MeV. Present measurements on the APEX RF gun at LBNL are less than 1 nA. It is expected that the natural dark current has a large effective emittance and most of it is collimated away at low energy. In particular, if the emission of dark current is uniform across the cathode at the full 400 nA, only 25 nA of dark current makes it to the undulator and DASEL kickers. Such a model is thought to be highly pessimistic, as the measurements of dark current have shown emission concentrated around the edge of the cathode, in which case essentially *all* dark current is collimated away before it reaches the kicker systems.

To achieve higher currents for DASEL (as for SuperHPS) and ensure the performance required for LDMX, a separate gun laser is used, which intentionally populates “dark current” bunches at a sub-harmonic of the gun frequency. These bunches are well separated from the primary beam bunches so they can be extracted downstream. The new gun laser would share the LCLS-II RF gun 46 MHz laser oscillator but would have a separate amplifier, UV conversion, and transport, all of which operate at much lower average power than the LCLS-II systems [18].

The desired beam emittance for the LDMX experiment is large enough so that the beam can be defocused to a large cross-section of roughly 4x4 cm. The desired beam emittance is many times (100-1000) that of the LCLS-II emittance (as well as the LCLS-II admittance, which is determined by the collimation system). This increase is accomplished using the ESA spoilers with a corresponding degradation of the beam current. A spoiler system increases the beam emittance and the beam energy spread.

Assuming an incoming, mono-energetic, 4-GeV beam, a simple 0.1 r.l. spoiler system increases the emittance to more than 300 mm, with more than 50% of the current within 0.5% of the incoming energy. In practice, the spoiler and downstream collimators are used to control the beam emittance and current at the LDMX detector. The spoiler system has been specified for beam current up to 100 times higher than that needed at the experiment (i.e., 55 W) to allow options for precise control and shaping of the electron beam at the experiment.

Table 1. DASEL electron beam parameters

Experiment Parameters	**LDMX-style**	**Super-HPS-style**
Energy	4.0 GeV (possible to upgrade to 8.0 GeV)	4.0 GeV (possible to upgrade to 8.0 GeV)
Bunch spacing	21.5 ns	5.4 ns
Bunch charge	0.04 – 20 e-	70,000 e- (10 fC)
Macro pulse beam current	0.1 – 150 pA	2 uA
Duty cycle	55% (600 ns out of 1.1 us)	55% (600 ns out of 1.1 us)
Beam norm. emittance (rms)	~100 um; < 1000 um	~1 um
Bunch energy spread	<1%	<1%
IP spot size	4 cm x 4 cm (rastering at 40 MHz could be used)	<250 um including jitter
Max beam power	0.5 W	5 kW
ESA Spoiler Parameters		
Charge reduction	0 – 99.99%	N/A
Emittance increase	1 - 1000x	N/A
Max beam power	55 W	N/A
Spoiler thickness	0 – 0.5 r.l.	N/A
Accelerator Parameters		
Macro pulse beam current	0 – 25 nA	2 uA
Beam norm. emittance (rms)	~1um; < 25 um	~1um; < 25 um
Beam admittance (edge)	<50 nm, defined by LCLS-II collimators	<50 nm; defined by LCLS-II collimators
Bunch energy spread (FWHM)	<2 %	<2 %
Bunch length (rms)	<1 cm	<1 cm
Max beam power	55 W	5 kW

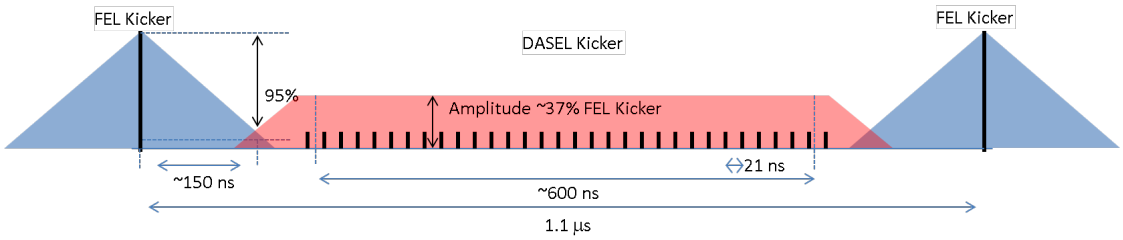

Figure 7. LCLS-II pulse structure showing primary pulses with 4x108 e- and dark current bunches from the gun with ~30 e- per bunch. The DASEL beam would require control of the dark current population with an additional seed laser and a spoiler/collimation system to deliver final current in the pA (for LDMX) to μA (for SuperHPS) range.

The LDMX benchmark requires limiting the average beam current to 5-to-30 pA for its first engineering run, increasing it to about 125 pA for an ultimate physics run. As noted, spoilers and collimators along the ESA beamline are used together with the secondary laser to carefully control the number of particles and the phase space of the e- arriving at the detector. LDMX requires a high suppression of off-energy electrons. It is expected that the ESA energy collimators are sufficient for this task.

3.2 Gun Laser and Integration with LCLS-II Laser Systems

The DASEL laser system is co-located with the LCLS-II laser systems in a laser room upstream of sector 0, approximately 60 m from the photoinjector. Sufficient optical table space is available for the DASEL laser system, as described in this section.

The LCLS-II laser system is based on a commercial laser architecture and operates with a 46.4 MHz master oscillator from which pulses are selected down to the nominal maximum repetition rate of the FEL of 0.928 MHz. The highest e-beam repetition rate at which DASEL could operate is set by the gun frequency of 185.7 MHz. To operate DASEL at this maximum repetition rate would require an independent laser oscillator/amplifier system and a timing and synchronization system running at 185.7 MHz, with many additional costs related to control systems and laser diagnostics. The most economical solution is for DASEL to operate at the 46.4 MHz repetition rate of the LCLS-II laser by splitting the oscillator before the LCLS-II amplifier and adding a separate amplifier and harmonic generation stages for DASEL. This solution reduces the cost of the laser system by a factor of 5, eliminates the cost of a separate timing system, and minimizes the optical table space required by DASEL, albeit at a 4-time reduction in overall data rate. The block-diagram of the DASEL laser system is shown in Figure 8.

Another factor to be considered in trying to minimize the cost and complexity of the DASEL laser system is the relaxed requirement in terms of the e-beam emittance, which translates into relaxed requirements on the transverse spatial and temporal profile of the laser beam, both of which have tight tolerances for the LCLS-II laser system.

The baseline photocathode material for LCLS-II is Cs2Te, which requires illumination by ultraviolet (UV) laser light at approximately 260 nm, for a few percent quantum efficiency (QE). Nonlinear crystals are used for fourth-harmonic-generation (4HG) stages from the fundamental laser wavelength in the infrared (IR) (~1040nm) to the UV. The few

femtoCoulomb bunch charge requirements of DASEL require only femtoJoules of UV energy on the cathode. However, higher energy pulses are required for practical reasons, such as beam transport losses, the ability to detect and align the beam, and the use of commercial diagnostics to monitor the beam. Furthermore, the efficiency of the 4HG process scales as the IR intensity squared, followed by the second harmonic intensity squared — approximately the IR intensity to the 4th power. The intensity of the laser can be increased by focusing into the harmonic conversion crystals; several practical factors, however, set a minimum pulse energy for efficiency of fourth harmonic conversion at approximately 20nJ/pulse, or ~1 W average power at 46.4MHz in the IR, with anticipated average power of ~1 mW in the UV. These considerations set the requirement for the DASEL laser amplifier, which is very conveniently available commercially from the same manufacturer as the LCLS-II laser system.

Another consideration for DASEL is the use of illumination by the “green” second harmonic of the IR laser at ~520nm. Cs2Te has a QE at 520 nm that is about five orders of magnitude lower than at 260 nm; but only a few milliWatts of average power would be needed to produce sufficient charge for DASEL; this performance could easily be produced by the IR system described above, with the added benefits of operating in the visible range (e.g., reduced overall complexity of the laser source, simpler and less expensive diagnostics, reduced beam-based damage of optics). The possibility of employing this scheme will be considered after the characterization and commissioning of the LCLS-II photoinjector, at which time the photocathode response to green illumination could be measured.

Two options are considered for the transport of the DASEL beam to the photocathode. The first option is to use the LCLS-II beam transport system, which is a ~60m long evacuated beam tube with relay-imaging optics, beam pointing stabilization, and inline diagnostics. The DASEL beam could be spatially offset from the LCLS-II beam in order to spatially separate the beams on the optical table adjacent to the photoinjector.

The second option is to propagate the DASEL beam to the RF gun using fiber optics. This option is not available for the LCLS-II laser beam because of the degradation of laser beam properties associated with fiber optic transmission of high intensity beams—e.g., phase dispersion, self-phase modulation, polarization dispersion, etc. Because of the significantly lower pulse energy and relaxed requirements on the temporal fidelity of the laser pulses for DASEL, fiber optics may be suitable. Although there are fibers designed for UV (260 nm) transmission, the cost, longevity, and impact on the laser characteristics are not well characterized. An alternative under consideration would be to transmit either the green (510 nm) or IR (1040 nm) to the photoinjector optical table and then perform the second and/or fourth harmonic conversion near the gun.

From the photoinjector optical table, the DASEL laser beam could be coupled into the photoinjector collinearly with the LCLS-II beam through the south-side window, or possibly through the north-side window, depending on physical interferences from other photoinjector systems (vacuum, cabling, etc.). A conceptual layout for the collinear option is shown in Figure 9.

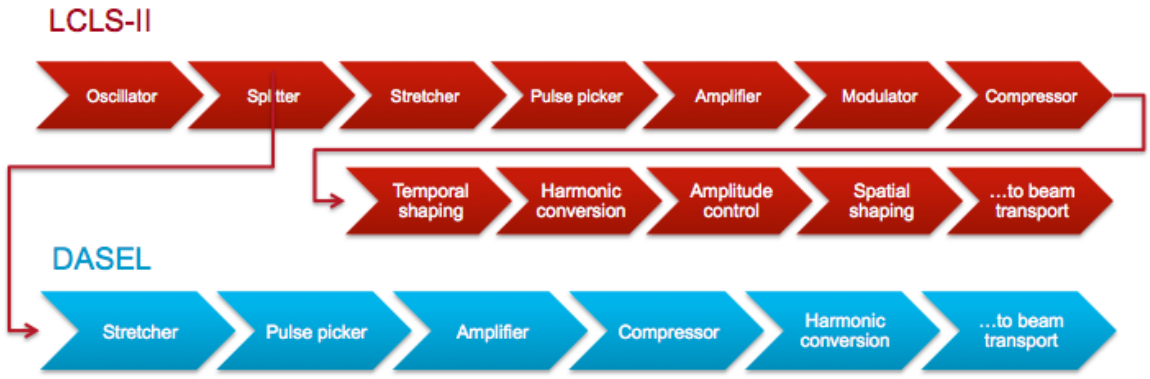

Figure 8. Block diagram of the DASEL and LCLS-II laser systems. The DASEL laser system uses a fraction of the light from the LCLS-II oscillator at 46.4 MHz, which is synchronous with the RF gun. The oscillator pulses are stretched in time, then can be down-selected by a pulse picker into a macrobunch to match the DASEL kicker, after which a commercial amplifier increases the oscillator pulse energy to 20-100nJ, sufficient to produce efficient UV at 260 nm after compression.

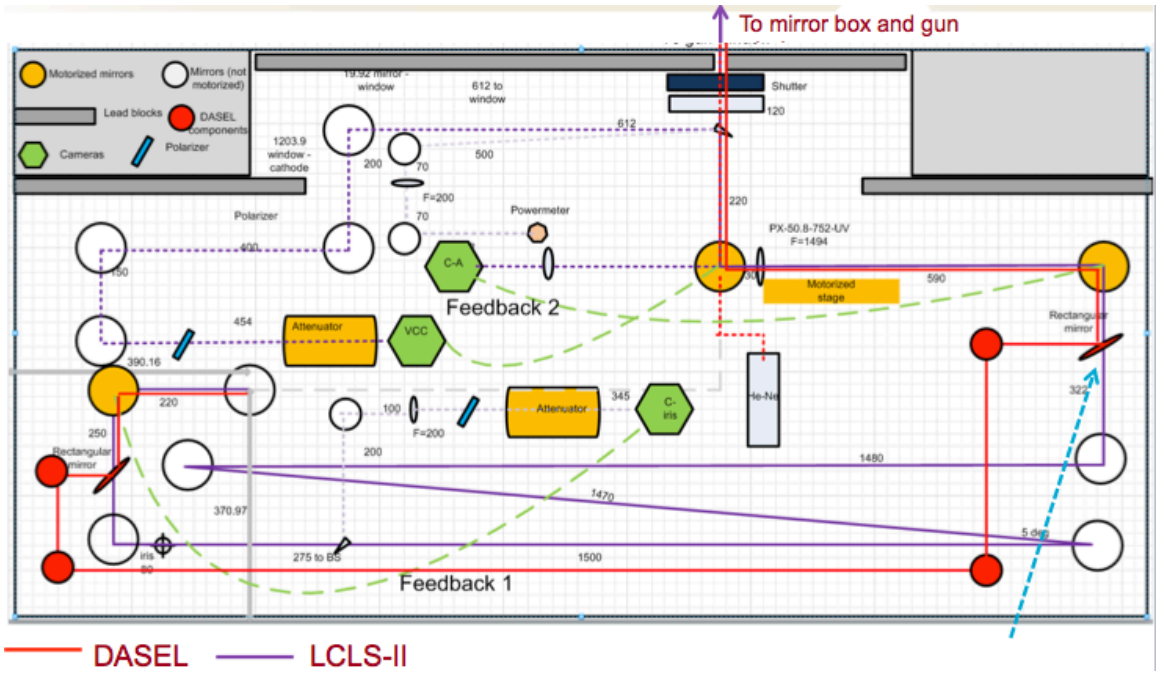

Figure 9. Conceptual layout of the photoinjector optical table layout showing one means by which the DASEL laser beam could be coupled co-linearly with the LCLS-II laser beam onto the cathode. The possibility of coupling the DASEL beam into the far-side of the photoninjector mirror box will also be studied.

3.3 DASEL Beamline from BSY Dump Line to ESA Line

The DASEL beamline connects the BSY dump line to the A-Line towards End Station A (ESA) as shown in Figure 10 and Figure 11. These figures illustrate the configuration of the LCLS-II beamline spreader at the end of the CuRF linac and in the BSY region; the location of the extractions to the HXR and SXR undulators; and the extraction to ESA for DASEL. The spreader is a complicated region with several beamlines running through a

65x65-cm cross-section, so that the DASEL beamline needs a detailed technical design to ensure efficient installation.

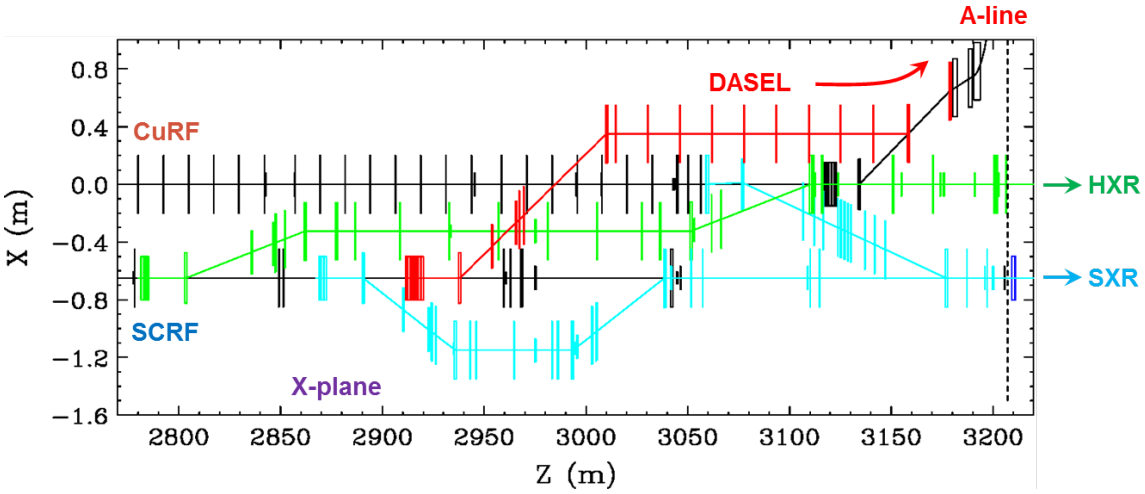

Figure 10. Top view of the LCLS-II spreader with the DASEL beamline. The beamline to the HXR undulator is colored green; the beamline to the SXR undulator is colored blue (including the link from the CuRF linac); the DASEL beamline is colored red; the elements colored in black belong to the CuRF linac, BSY dump line and A-line; the BSY dump is shown as a dark blue box behind the face of BSY muon wall (vertical dash line).

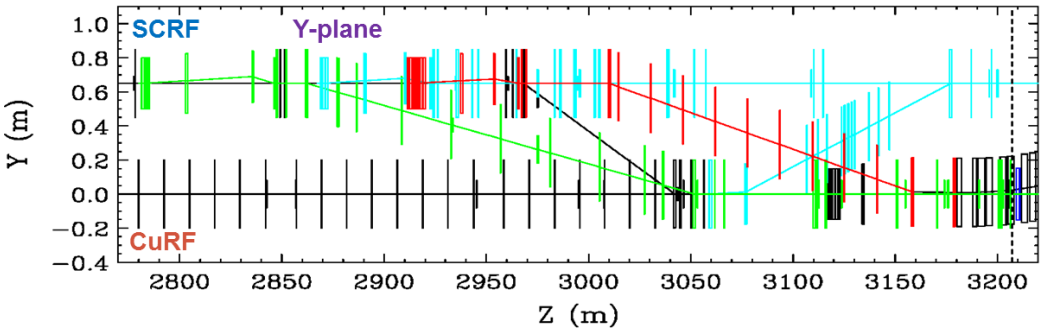

Figure 11. Side view of the LCLS-II spreader with the DASEL beamline (colored red).

To ensure parasitic beam operation to the LCLS-II FEL, the DASEL vertical kicker is placed downstream of the HXR and SXR FEL kickers and septa, at the bypass height upstream of the dump line vertical bends. The kicker consists of seven one-meter sections that direct the beam into a two-hole Lambertson septum magnet. A small vertical kick is used to select a septum hole with strong horizontally deflecting field (for DASEL bunches) or with no field (for main bunches passing to BSY dump). After the septum, the DASEL line makes a horizontal cross-over above the HXR and CuRF linac lines connecting to a rolled DC-bend magnet located 65 cm above and 35 cm to the left of the CuRF linac. This magnet provides horizontal and vertical bending directing the beam downward at a shallow angle, and parallel to the CuRF linac, towards the second rolled DC-bend which connects the DASEL line with the A-line. Eleven quadrupoles and two weak vertical dipoles are included to provide the beam focusing and compensation

of kicker orbit and dispersion. A third rolled DC-bend is required in the beginning of the A-line for compatibility with a future connection of the A-line to the LCLS-II HXR line. The DASEL optics functions are shown in Figure 12. The optics of the A-line, matched to DASEL. is shown in Figure 13.

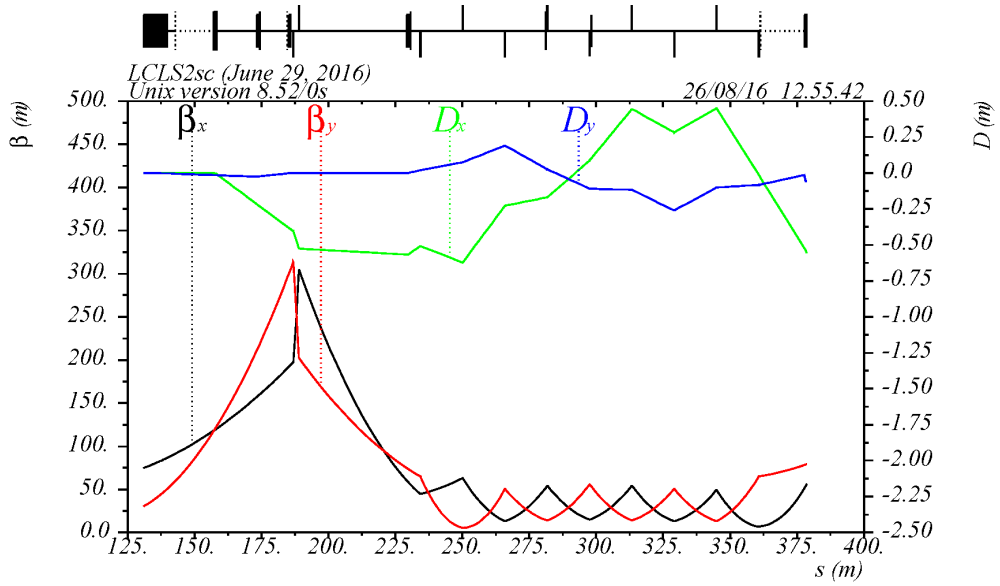

Figure 12: Optics functions of the DASEL beamline

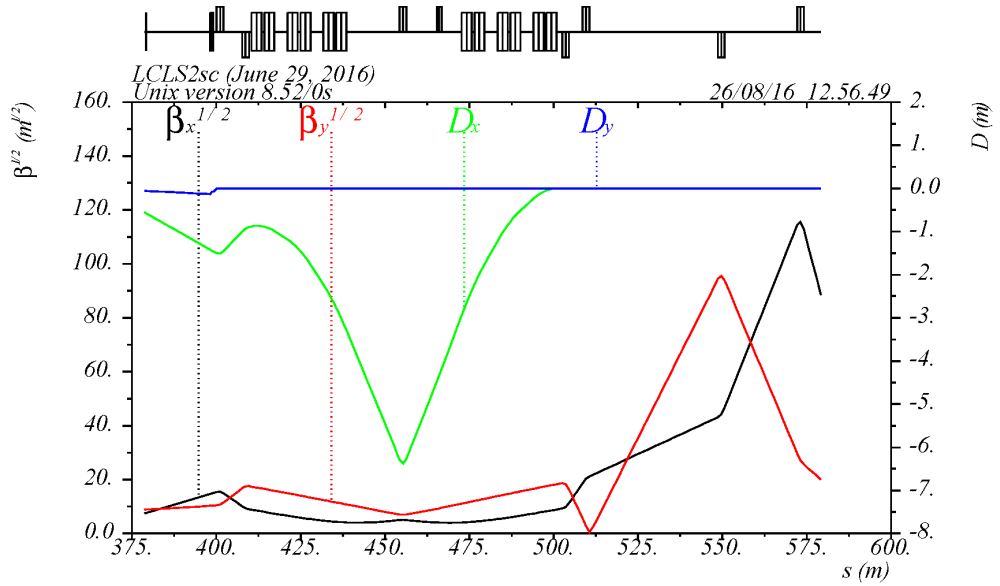

Figure 13: Optics functions of the A-line matched to DASEL.

The DASEL beamline is designed to make use of the magnets available at SLAC and existing magnet designs, wherever possible. These include the available PEP-II bypass dipoles 1.0D22.625 and 1.0D38.37 and the available quadrupoles 2Q4W. The septum magnet is of a new design (0.625SD38.98) developed for the LCLS-II HXR and SXR lines. The kicker design is under development, based on the LCLS-II FEL kicker design. The parameters of the DASEL magnets at 4 GeV beam energy are listed in Table 2,

including the required new bend magnet in the A-line. Photographs of the existing 2Q4W quadrupole and 1.0D38.37 dipole at SLAC are shown in Figure 14.

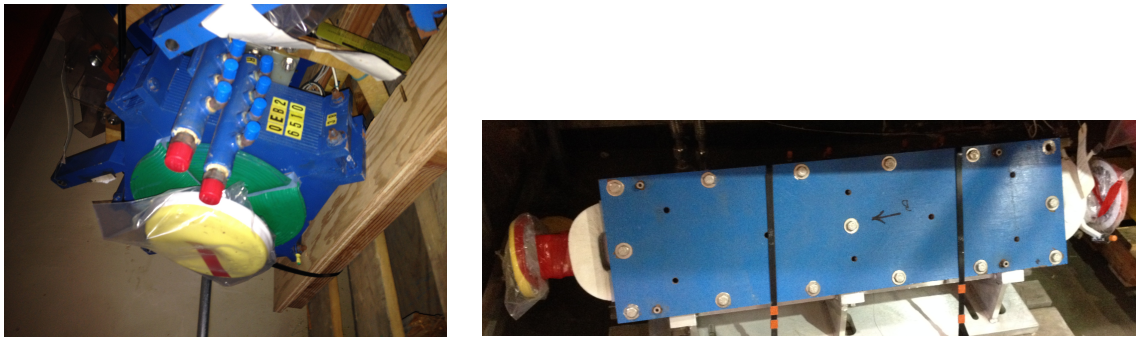

Figure 14: Photos of 2Q4W (left) and 1.0D38.37 magnets recovered from SLAC for use in LCLS-II and DASEL.

DASEL Beam Stay Clear (BSC), consistent with LCLS-II collimation, and DASEL beam size for a specified normalized emittance of 25 μm-rad and energy spread of ± 2% are shown in Figure 15. The proposed DASEL magnets provide adequate aperture and magnetic field at 4 GeV beam energy. With a modest kicker upgrade and two additional 2Q4W quadrupoles, the beamline is compatible with 8 GeV beam. The quadrupoles require nine independent power supplies and the septum and five bend magnets need five power supplies. DASEL beam diagnostic and correction system is shown in Figure 16. It includes one BPM to control the kicker orbit, three profile monitors, and five dipole correctors along with trims on four dipoles for orbit correction. Two additional BPMs are included as part of Machine Protection System (MPS).

Table 2: Magnet parameters.

	Quantity @ 4 GeV	Design	Aperture (mm)	Max. field @ 4 GeV	Availability
Quadrupole	11	2Q4W	53.8	14.82 kG	Existing magnet
Kicker	7	0.787K35.4	10	12.8 Gm per kicker	New, based on LCLS-II
Septum	1	0.625SD38.98	15.9	1.85 kGm	New, based on LCLS-II
Rolled bend	3	1.0D38.37	25.4	2.02 kGm	Existing magnet
Weak vert. bend	2	1.0D22.625	25.4	0.38 kGm	Existing magnet

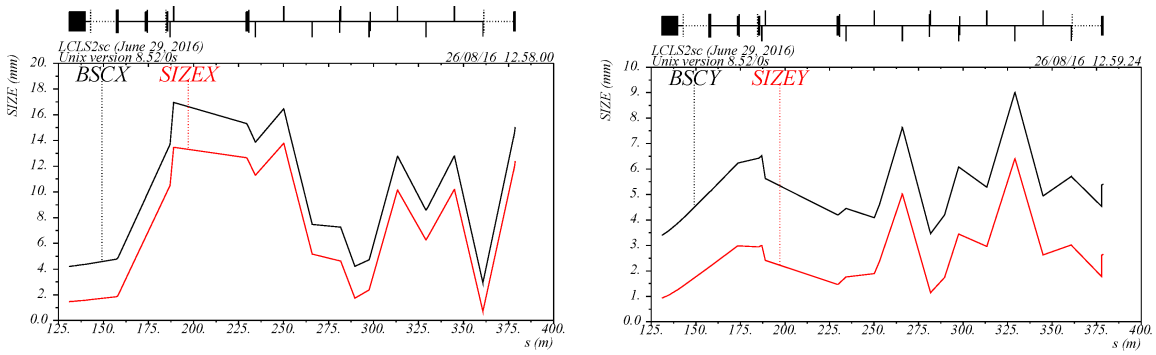

Figure 15: **Beam Stay Clear (BSC) and full beam size in DASEL beamline (left, horizontal; right, vertical). BSC is determined assuming admittance of 65 nm-rad, ± 2% energy spread and 2 mm orbit, consistent with LCLS-II BSC. Full beam size is defined as: $3\sqrt{\beta\varepsilon} + |\eta|\Delta p / p$ for normalized emittance of 25 μm-rad and $\Delta p/p$ = 2%.**

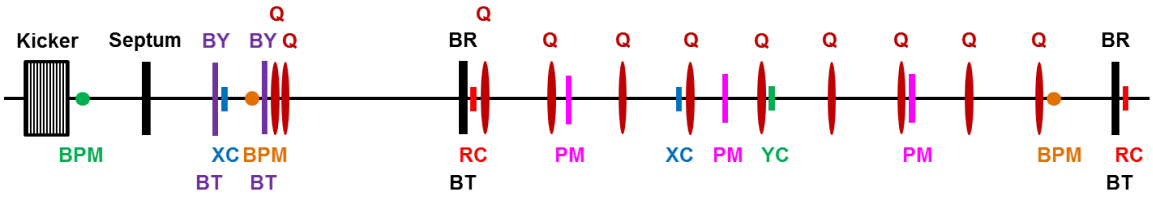

Figure 16: **Schematic of the diagnostic and correction system for the DASEL beamline. It shows the DASEL kicker; the Lambertson septum magnet; 2 weak vertical bends (BY); 2 rolled bends (BR); 11 quadrupoles (Q) for 4 GeV beam; a BPM for kicker orbit control (colored green); 2 MPS BPMs; 2 horizontal (XC), one vertical (YC) and 2 rolled (RC) dipole correctors; 3 profile monitors (PM); and 4 bend trims (BT) on the main bends.**

The LCLS-II spreader is a congested region containing several beamlines—including the DASEL line—where most magnets share a 65-by-65-cm cross-section. To avoid interference with the LCLS-II lines, the DASEL magnets are separated from magnets on the other lines longitudinally, both horizontally and/or vertically. An example of the area in the middle of the DASEL cross-over is presented in Figure 17, where DASEL magnets BYDCA1, BYDCA2, QDCA1, QDCA2 are shown along with the HXR, SXR and CuRF linac quadrupoles QSP7H, QSP5S and Q30201 and dump line vertical dipole BYSP1D. A preliminary analysis of the spreader tunnel indicates possible obstructions within the existing infrastructure (e.g., cable trays, cooling lines). These, however, will be cleared for LCLS-II or can be resolved for DASEL. The complete analysis requires a detailed 3D engineering design.

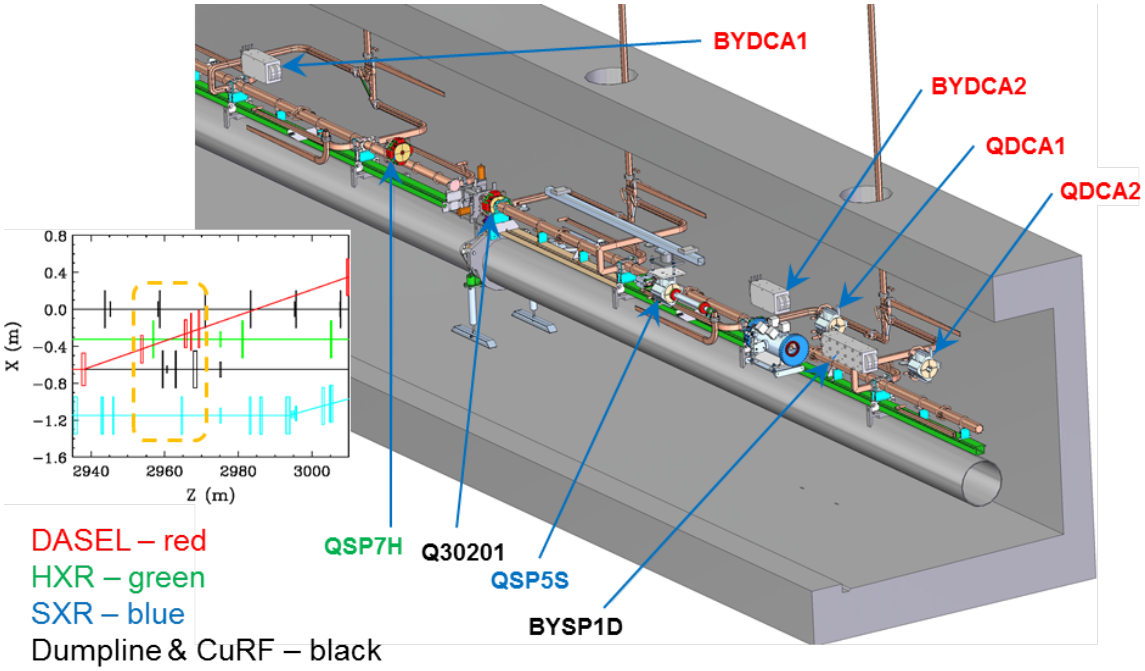

Figure 17. **3D view of the spreader in the middle of DASEL cross-over showing DASEL weak dipoles BYDCA1, BYDCA2 and quadrupoles QDCA1, QDCA2; HXR quadrupole QSP7H; SXR quadrupole QSP5S; CuRF linac quadrupole Q30201; and dump line vertical dipole BYSP1D.**

3.4 DASEL Kicker and Septum

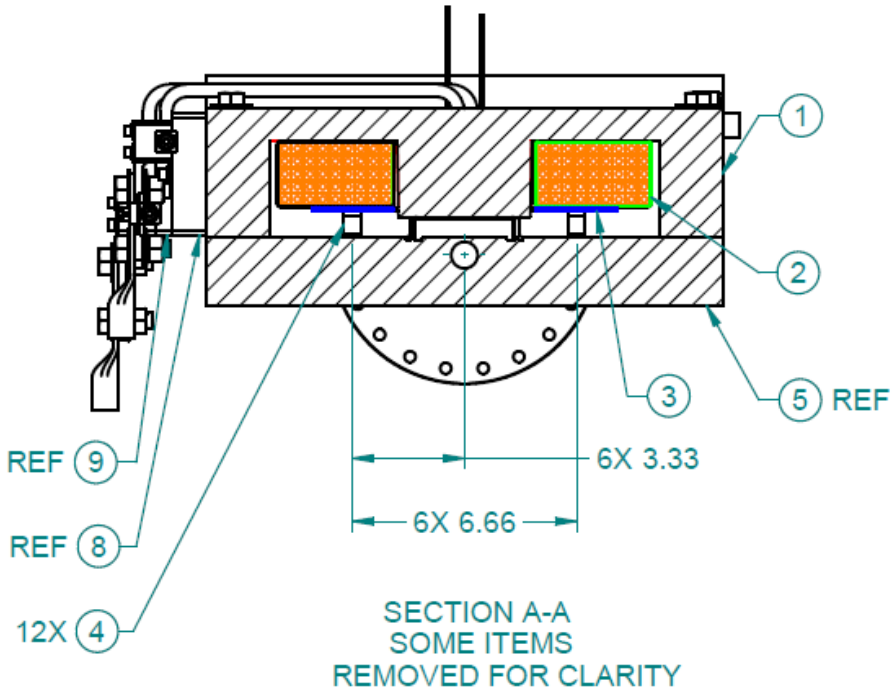

Figure 18. **The LCLS-II 0.625SD38.98 septum dipole cross section. The small central hole on the lamination transports un-kicked beam. Kicked beam is deflected horizontally in the rectangular gap between the spacers.**

The DASEL beam diversion system consists of a septum magnet and a vertical deflecting magnetic kicker. The kicker/septum combination diverts beam towards the DASEL beamline. When the kicker is not energized, the beam traverses the zero field region of the septum magnet and is transported to the LCLS-II dump.

The septum magnet is a duplicate of the LCLS-II HXR and SXR Lambertson septa magnets. A drawing of the magnet is shown in Figure 18. The separation between the center of the undeflected and deflected beam channels is 15 mm. The required integrated magnetic field of the kicker to achieve the 15 mm separation is ~90 Gm.

The LCLS-II pulse structure and profiles of the FEL kickers and proposed DASEL kicker are illustrated in Figure 7. The kicker operates with a pulse rate of 929 kHz and a flat-top of roughly 600 ns. The DASEL kicker operates at the same rate as the LCLS-II kickers but at a lower amplitude and looser tolerance than the FEL kickers. The LCLS-II kickers have a 90% rise/fall time less than 300 ns [19], so that, allowing for the DASEL kicker rise/fall, roughly 600 ns of "dark" current between successive primary bunches spaced at 1.1 μs could be extracted toward ESA.

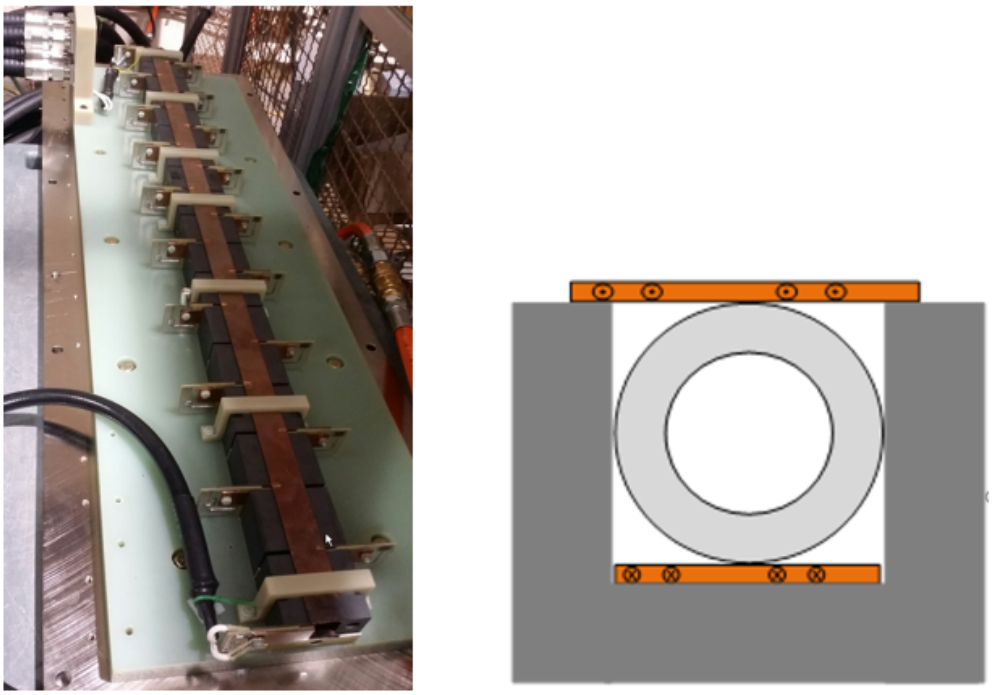

Figure 19. Left: Prototype lumped-element kicker magnet. Right: cross-section of magnet beampipe, ferrite, and bus bars.

The kicker is based on a design in development for the LCLS-II spreader kicker. A ferrite loaded magnet topology has been selected to reduce the amount of energy transfer to the magnet per kick, thus reducing the kicker's average power requirements. With this design, drive voltages can stay safely in the operating range of commercial MOSFETs. The magnet consists of serially connected L-C segments that approximate a transmission line. The inductive part of each section is made up of ferrites, gapped to accommodate the beam aperture. The capacitive part of each section is realized via

discrete capacitors mounted in parallel on a printed circuit board. The capacitance can be easily adjusted to tune the magnet to the characteristic transmission line impedance of the system. Two copper bus bars provide conduction paths for supply and return current. Each magnet is composed of 18 segments. To obtain the required magnetic field and limit average power, the kicker system is comprised of seven kicker magnets. Each one-meter magnet section contains an extruded ceramic metalized beam pipe to isolate the vacuum and provide uniform beam impedance. Depictions of a prototype magnet and a magnet cross-section are shown in Figure 19.

For LCLS-II, each kicker system is comprised of a DC supply, transmission line cables, a lumped element magnet, and resistive load, as shown in Figure 20

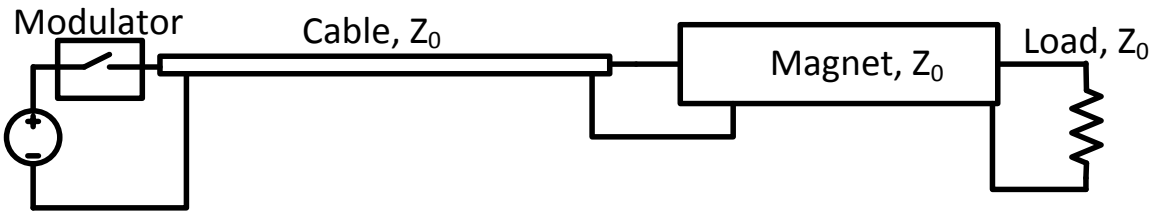

Figure 20. Conceptual diagram of an LCLS-II kicker system.

The transmission line design allows for a cable run long enough to locate the DC supply and modulator above the tunnel in the SLAC klystron gallery for ease of maintenance. For LCLS-II, it is critical that the pulse be as short as possible such that the remnant field following the pulse has the maximum amount of time to settle to zero, ensuring the next beam bunch is not perturbed. DASEL's settling requirement is significantly reduced. Thus, it is possible to extend the DASEL kicker pulse length by increasing the conduction time of the modulator MOSFETs. The downside of this approach is that the load power and MOSFET losses increase proportionally with pulse width. To compensate for this effect, the kick strength of each section must be reduced, where power losses scale inversely with the square of the kick strength. The LCLS-II one-meter prototype magnet and test stand were used to make preliminary measurements of the DASEL kicker pulse. Below, Figure 21 shows a three-pulse burst of a field strength and duration near the DASEL requirements.

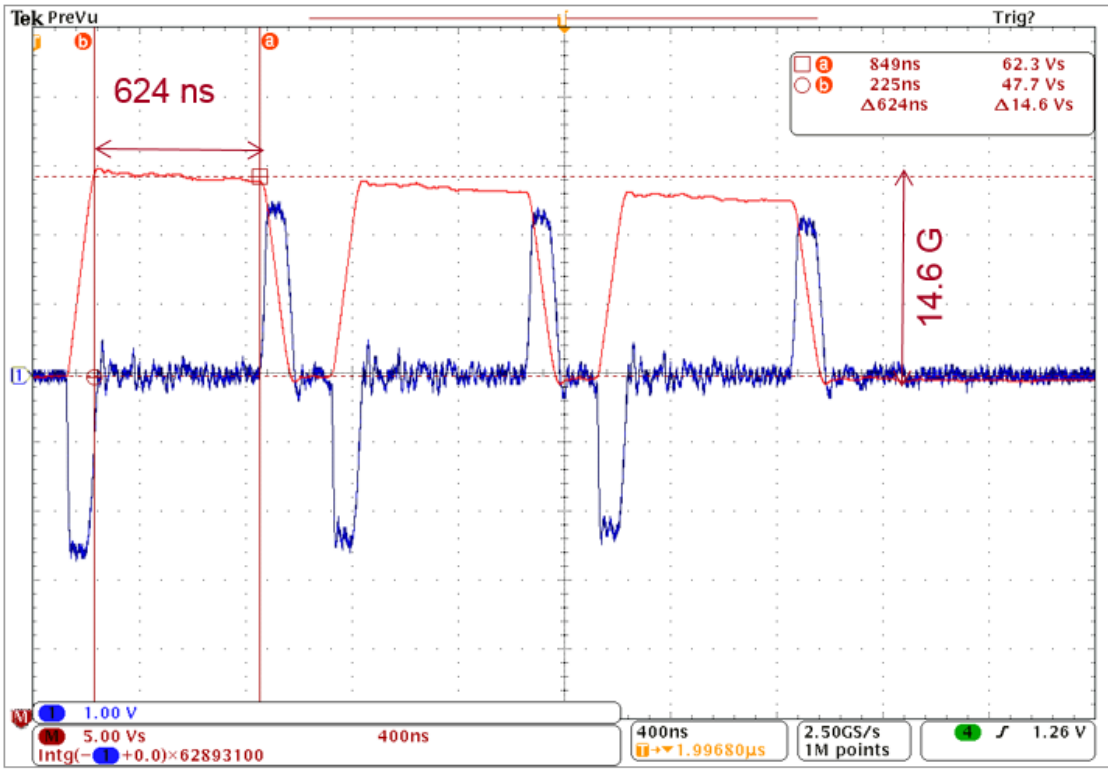

Figure 21. Measurements taken on LCLS-II prototype test stand. The blue waveform is taken from a Bdot probe within the magnet. The red waveform shows an integration of the Bdot signal yielding the integrated magnetic field.

Additional testing using the LCLS-II prototype test stand will be necessary to ensure that the increased pulse width does not add additional complications and to improve upon pulse flatness and repeatability.

Each magnet section takes approximately 100 ns to fill with field. To reduce cost, it should be possible to power multiple magnets with one modulator, cable, and load at the expense of increasing the magnet fill-time and slightly increasing power losses.

There is an upgrade path for the kicker should 8 GeV be required. The field can easily be doubled by increasing the driver voltage proportionally. However, this does lead to prohibitive power loss, especially in the load and driver transistors. This effect can be accommodated by paralleling two loads and doubling the number of driver transistors. While this solution shifts the design away from the LCLS-II design, it is a small development effort.

3.5 A-Line, Spoiler/Collimator System, and End Station A Infrastructure

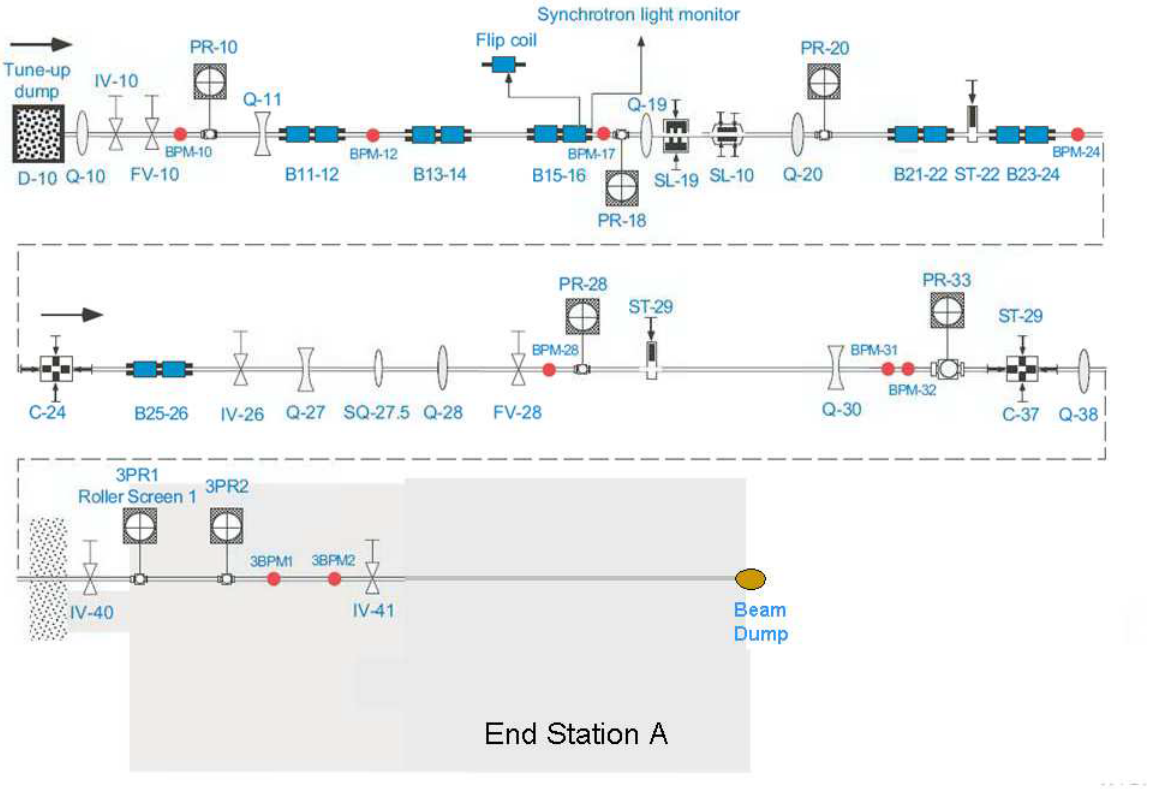

Figure 22. Layout of devices in the A-line. PR-10 and SL-10 together with the 2 four-jaw collimators C-24 and C-37 provide the spoiler and collimator system for controlling the beam profile. ST-22 and ST-29 are two beam stoppers, which, together with the DASEL kicker, are included in the PPS system to allow access to the ESA area housing.

The A-line, which transports beams from the central part of the Beam Switch Yard (BSY) towards End Station A (ESA), was configured in its present form about 20 years ago to support high-energy and high-power beam operations for the E-158 experiment. A schematic is shown in Figure 22. The A-Line starts with quadrupole Q10 and ends with the vacuum valve IV-41 at the entrance of ESA. In 2013, the End Station Test Beam program (ESTB) was established at SLAC to provide particle beams for detector R&D experiments in ESA. That program makes use of the LCLS normal conducting Linac beams. The A-Line is set up to transport either the primary LCLS beam or a spoiled and collimated reduced number of electrons (secondary electron beam) from the LCLS beam into ESA. ESTB has operated with the full range of available LCLS-beams: electron beam energies between 2.5 GeV and 16.5 GeV and bunch charges between 20 pC and 280 pC.

Presently, secondary electron beams are generated by steering selected LCLS bunches onto a 6-mm copper target in the BSY. Electrons are scattered and the resulting electron beam has a wide energy spread, which is then transported through the A-line into ESA. The thickness and material of the target are chosen appropriately to reduce the number of hadrons generated in the electron-target interaction to negligible levels. Additional

spoilers, such as the profile monitor PR-10, are available to further diffuse the electron energy spread without generating a significant number of other particles. The A-Line bend magnets are set to the particle energy required by the experimenters in ESA. Secondary particle beams have been delivered from 2 GeV up to the full-LCLS beam energy. A multi-collimator system in the A-line is used to control the number of electrons per pulse. The momentum slit SL10 restricts the accepted beam energy spread from about one percent to less than one part per million. The four-jaw collimators C-24 and C-37 are used to reduce the geometrical spread of the accepted beam reaching End Station A.

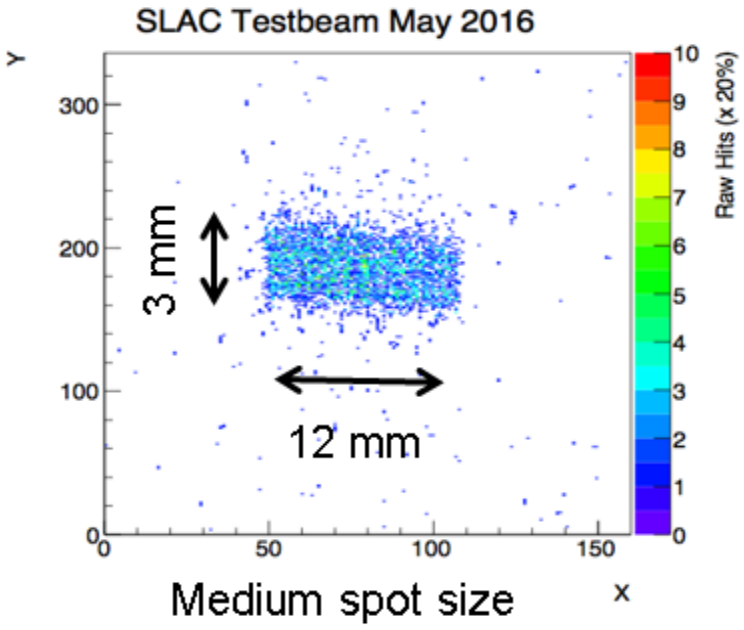

Figure 23: ESTB delivering a medium size spot with clean edges.

Figure 23 shows a typical beam spot generated by C-24 and C-37 of 3x12 mm which was measured during a recent silicon detector test. For this experiment, the average electron number was set to about 25 electrons per bunch. Other spot sizes, larger or smaller, can also be selected. In its present configuration, a fixed collimation system limits the maximum spot size in ESA to about 25x25 mm, which can be changed for LDMX to allow larger spots.

Figure 24 shows another example of secondary beams delivered to ESA, this time highlighting the A-Line's capability to finely tune the average electron rate per bunch.

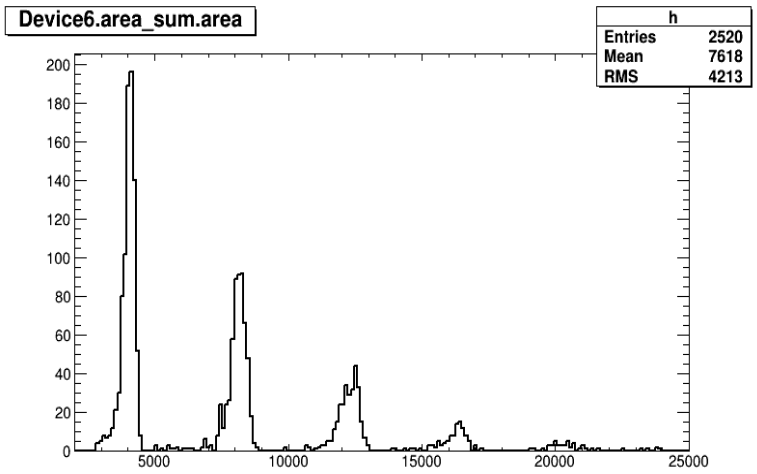

Figure 24. ESTB delivering 1 to 5 single electrons per bunch. Shown are the measured energy depositions of individual 3GeV electrons in a calorimeter. The first peak, at around 4,000 counts, had one electron per bunch, the second at 8,000 counts had two electrons per bunch, and so on.

End Station A is one of the original experimental halls built in the 1960s. It is about 60 m long and 40 m wide, with a ceiling height of about 20 m. The building has 50-ton crane coverage throughout the building. Figure 25 shows a rough layout. The A-Line beam enters ESA from the left side and traverses the building. IV-41, the vacuum valve mentioned above, is just to the left of the first red marker. The leftmost and rightmost markers show possible locations of the LDMX detector within the building. The beam dump is located at the east wall, just to the right of the rightmost marker. The free space available at the rightmost location is approximately 8 m along the beam axis. Beam height is at 205 cm above the concrete floor. Electricity, low conductivity cooling water, and pressurized air are readily available anywhere in ESA. Multiple cable paths already exist from the experimental areas to the Counting House. A wide selection of high voltage, signal and Ethernet cables are already installed.

During beam operation, ESA is secured with a Personnel Protection System (PPS) which prevents access. For the few secondary particle beams, as required for LDMX, typical access time from beam operation off to entry into ESA is about two minutes; the beam can be turned back on within about three minutes after access has ended.

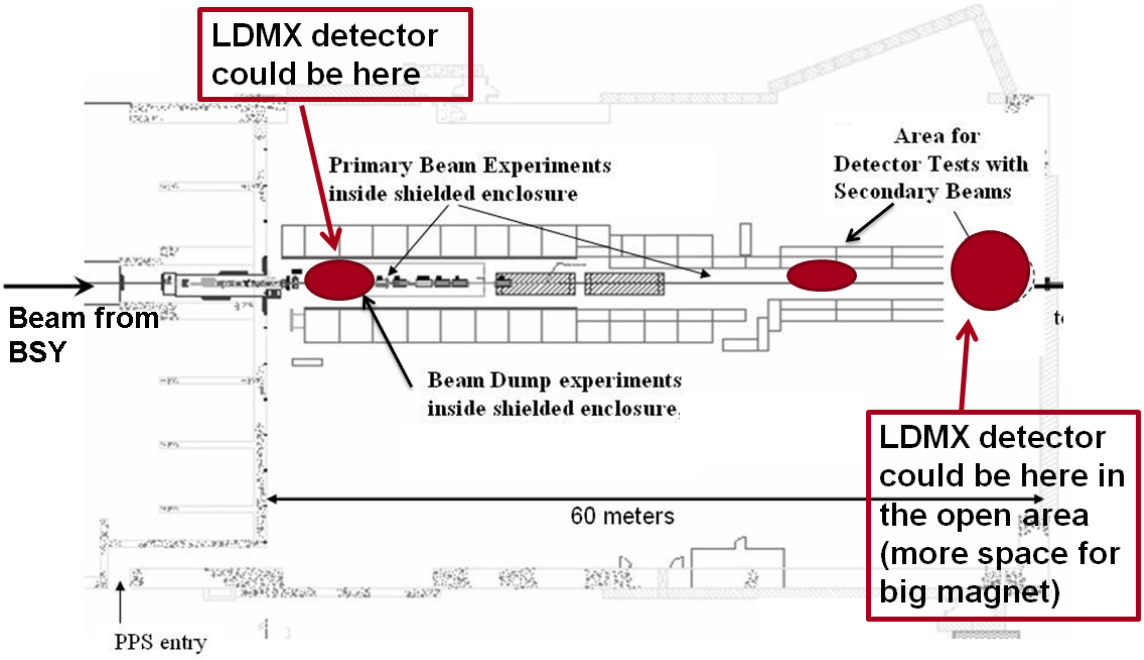

Figure 25. End Station A with possible locations for LMDX indicated.

3.6 Electron Beam Diagnostics and Tuning

The nominal DASEL bunch charge is too low to measure with standard diagnostics, such as BPMs. The beamline tuning is done with a special tune-up operating mode using low rate (1 ~ 10 Hz) of the LCLS-II primary beam. The primary beam can be extracted on pulses with the SXR and HXR undulator kickers turned off and the DASEL kicker timing shifted by 500 ns. In tune-up mode, the beam is stopped before it reaches the LDMX detector to prevent high charge bunches from damaging the detector electronics. Two BPMs are also used to provide a very fast MPS signal to halt the DASEL kicker in case errant high charge bunches are extracted unexpectedly.

To tune and align the beamline, three profile monitors are located along the length – see Figure **16**. These are placed to confirm the dispersion, phase advance, and overall match of the DASEL beam before it enters the ESA beamline.

In addition, the DASEL beamline has beam loss detectors along the length of the beamline — two Average Current Monitors (ACM) and two BPM striplines. The ACMs are part of the Beam Containment System (BCS) and Machine Protection System (MPS) but are also used to measure the DASEL current upstream of ESA. These systems have resolution down to 10 nA. The DASEL current is maintained using this signal to feedback to the source laser.

DASEL commissioning begins after the LCLS-II stably transports beam to the BSY Dump past the DASEL kicker. At that point, LCLS-II bunches are extracted to tune the DASEL beamline and ESA. After the beamlines are configured, the DASEL laser and ESA spoiler and collimator system are set up. The LCLS-II BCS Average Current Monitors (ACMs) have the resolution to detect 10 nA of dark current between the primary LCLS-II bunches at 929 kHz or 100 pA, when averaging without the LCLS-II

beam. The initial setup of the laser is performed without the LCLS-II beam to establish 10~25 nA of current. The injector ACM is then used to maintain this level as the LCLS-II beam is re-established. The DASEL ACMs are used to verify the current extracted by the kicker; then the ESA spoiler and collimator system are configured.

The final tuning of the ESA spoiler and collimation system is based on signals from the LMDX detector.

3.7 Radiation Protection

The DASEL beamline directs low-current beam from the LCLS-II into End Station A with a kicker system installed downstream of both the Hard (HXR) and Soft (SXR) X-Ray beamline kicker systems. There is no provision for beam from the LCLS-I copper Linac.

DASEL has a preliminary design for the required safety systems based on analysis by the Radiation Physics Group and discussions with the LCLS-II safety system designers. The design incorporates DASEL safety systems into the planned LCLS-II systems and uses almost entirely components that are identical to those already used elsewhere or those being fabricated for LCLS-II.

3.7.1 DASEL Layout

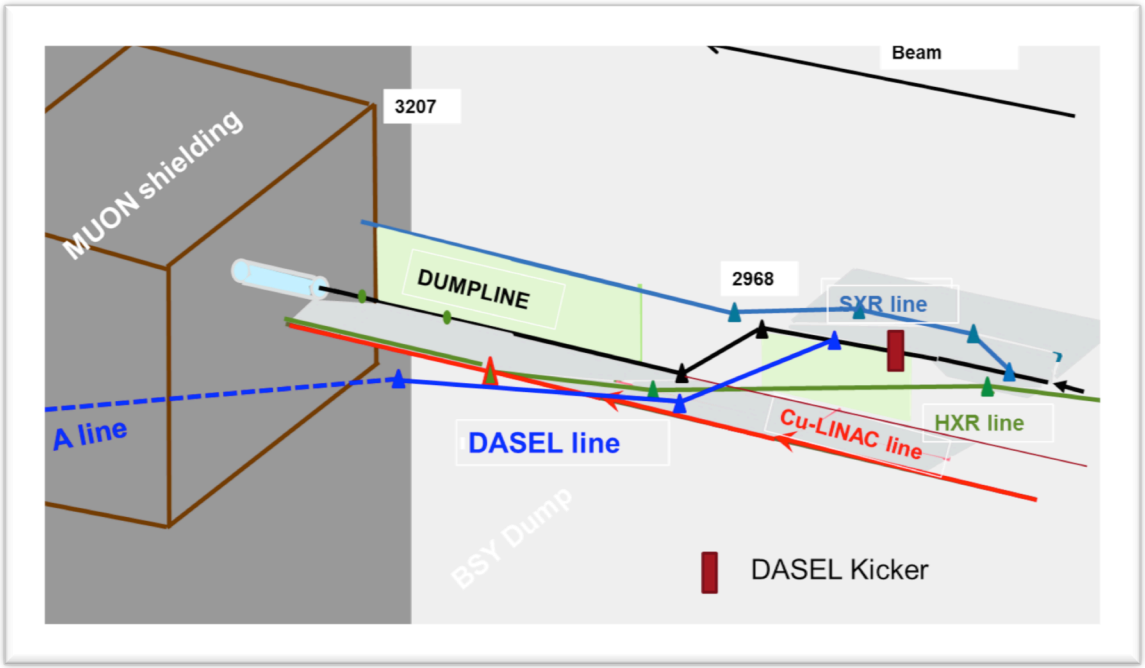

Figure 26. Radiation safety sketch of the beamlines in the BSY.

3.7.2 Personnel Protection System Requirements

The Personnel Protection System (PPS) must allow access to End Station A (ESA) during operation of either the superconducting (SC) LCLS-II Linac or the normal conducting copper LCLS-I Linac. In the event of access to the LCLS Beam Transfer Hall

(BTH), the DASEL beam is shut off. There is no need to allow DASEL beam operation during BTH access.

PPS requires three stoppers to prevent beam from reaching ESA during personnel access. These include two existing stoppers in the transfer line to End Station A and the DASEL kicker and septum. Any PPS fault trips off the LCLS-II beam. The current ESA PPS permits, control, and status feedback are unchanged.

3.7.3 Beam Containment System Requirements

The Beam Containment System (BCS) must limit the allowed beam power into End Station A (ESA). The DASEL BCS is an extension of the LCLS-II BCS and any BCS fault trips off the LCLS-II beam. Protection is provided by two (three) Average Current Monitors (ACM) in the DASEL beam line. The standard LCLS-II ACMs have a trip point that is adjustable over the range of 1 μA – 300 μA averaged over 25 μs. For the lower power DASEL beam, the ACMs are modified for higher gain with a trip point adjustable over the range of .01 μA – 3 μA averaged over 25 μs. The ACMs are set to trip at 100nA.

In addition to the ACMs, the BCS system includes Beam Point Loss Monitors (BPLM) and Beam Line Loss Monitors (BLLM). There are two BPLMs on each of two existing ESA collimators. The response time of the BPLMs is 100 μs. Two pairs of BLLMs are installed in the upstream and downstream ends of the ESA inner tunnel. Their response time is 600 μs.

Once the LDMX experiment is installed, two additional protection collimators must be installed around the LDMX dipole magnet. These must also be equipped with Burn Through Monitors interlocked to the BCS.

The BCS also contains four existing Beam Shut-Off Ion Chambers (BSOIC) around the ESA. A BSOIC trip causes the ESA PPS stoppers to go in. If any of the ESA PPS stoppers fails to activate, there is a PPS fault which trips off the LCLS-II beam.

3.7.4 Machine Protection System Requirements

The Machine Protection System (MPS) protects components of the DASEL beam line from damage. The DASEL MPS is an extension of the LCLS-II MPS, but any DASEL MPS fault trips off the DASEL kicker and puts in the stopper in front of the experiment. The MPS system monitors the BCS devices, such as ACMs, BPLMs and BLLMs. It has trip thresholds set low enough that the MPS should always trip before the BCS does. In addition, the MPS uses fast signals from the BPMs and shorter integration times from the protection devices to provide a faster response than that of the BCS. The MPS can also be tripped by temperature readouts, by fast and slow vacuum valves, and by a signal from the experiment. Figure 27 shows a rough schematic layout for the DASEL BCS and MPS systems.

If any protection device or BPM detects current 100 μs after the kicker has been turned off, a BCS fault is generated and the LCLS-II beam is turned off.

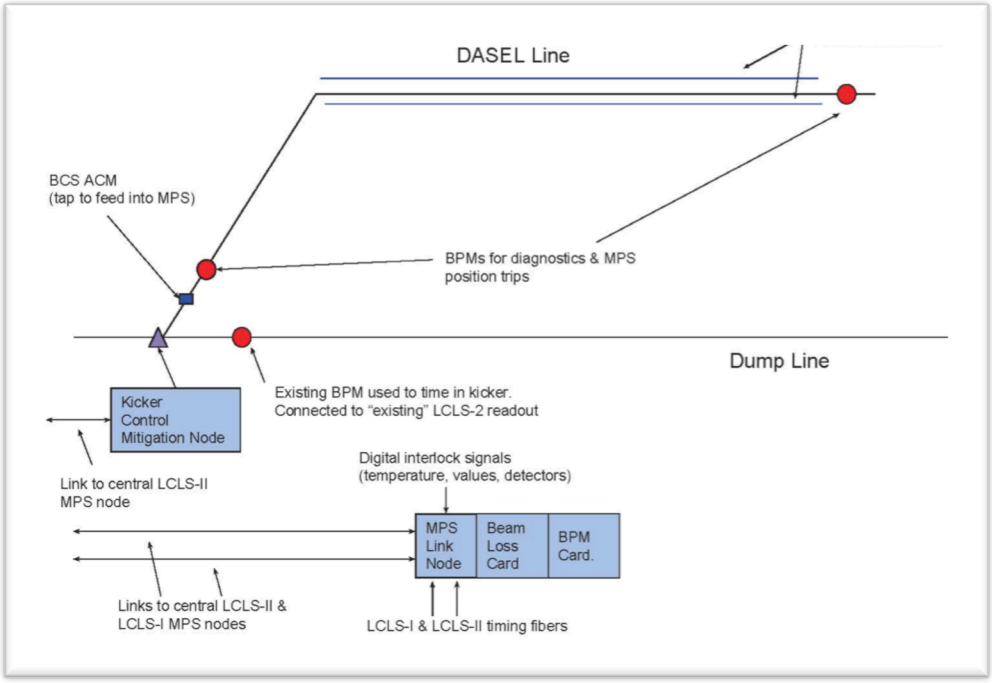

Figure 27. Schematic layout of MPS and BCS systems for DASEL

4 Project Management, Costs, Personnel, and Schedule

The timeline is set by the LCLS-II construction and installation schedule, as illustrated in Figure 28. Areas in the BSY are optimally accessed during LCLS-II's 12 month shutdown period, June 2018–June 2019. LCLS-II plans to send beam through the BSY in April of 2019, making that the effective deadline for DASEL installation. To meet this schedule, DASEL components need to be fabricated beginning in FY 2018.

After the LCLS-II commissioning is complete and operation begins, there are, as of now, no planned shutdowns when the DASEL beamline could be conveniently installed. Nonetheless, as the LCLS-II operations plan develops, short shutdowns are anticipated for repair or maintenance, which would allow DASEL to install items such as the kicker and laser. Traditionally, LCLS has shut down for 4 to 6 weeks in the summer and for 2 weeks at the end of the year.

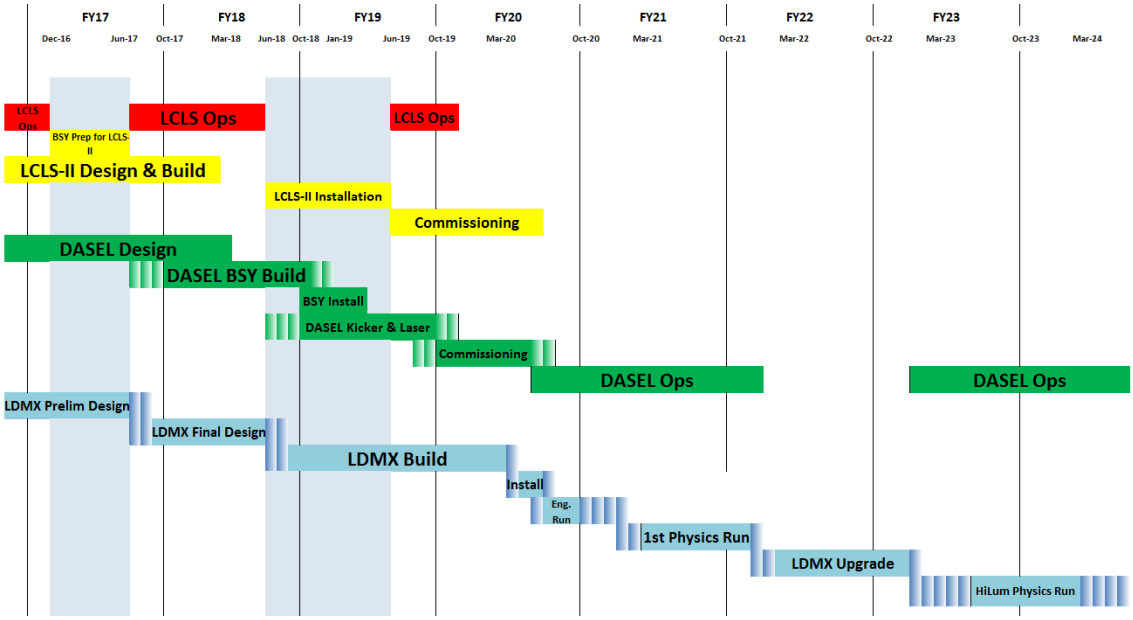

Figure 28. The current SLAC schedule for LCLS operations and LCLS-II design, fabrication and installation. To be ready for installation in BSY during the January-June 2019 period, DASEL construction funding has to be in place in FY 2018.

ESA has been selected as the optimal location for the initial DASEL experimental area. ESA is served by an existing, well-understood beamline that already incorporates a spoiler, momentum selection, collimation, and a beam shaping system. The ESA housing itself has beam containment (BCS), personal protection (PPS), and a beam dump system appropriate for handling beams of the power under consideration for DASEL, as well the infrastructure required to install and run the experimental program (crane coverage, connection to an experimental control room, etc.). The disadvantage of ESA is that SLAC's long-term plan calls for its conversion to a photon science facility sometime in the latter half of the next decade. The high-impact experiments, such as LDMX and potentially a SuperHPS experiment, should be able to be completed within the required time frame. Moreover, a DASEL transfer beam line to the entrance of the A-line may serve the photon science community later.

Figure 10 shows the current beamline design. It has 3 strong bends, 2 weak bends and 11 quadrupole magnets, along with the kicker and septum, in a 250-m long beamline. These components and the low intensity/high-repetition-rate source laser set the scale of the project. An initial cost estimate for DASEL has been made and is described below. As no devoted DASEL design funding yet exists, this estimate has been made by compiling component and labor costs estimated for LCLS-II by the LCLS-II engineering team. We envision FY 2017 as a pre-project period, where a funded DASEL design study produces a complete engineered design together with a quantified, defensible estimate of the cost. Project funding would need to begin in FY 2018 so that longer lead time items can be ready for the LCLS-II installation window.

4.1 DASEL Design Study

The project design is divided into three phases: conceptual design, preliminary design and final design, where final implies “ready-to-build.” The goal of the FY 2017 DASEL design study is (1) to bring the entire concept from the current “conceptual design” phase to the “preliminary design” phase; (2) to bring the design of the beamline connecting the kicker to the A-line to the final design phase; and (3) to have a reviewable cost and resource-loaded schedule so that acquisition and manufacturing can begin in October 2017. Given the profusion of transfer lines in the BSY (see Figure 10), it is important that an engineered 3D CAD layout of the proposal be provided as early as possible to assure stakeholders that the new beamline does not adversely impact LCLS-II operation. Informal discussions indicate that four-person months of a CAD designer and a one-person month of engineering support for magnet supports and magnet infrastructure would satisfy this goal. Figure 29 and Figure show isomorphic and plan views in the region where the DASEL beamline crosses over from the SC LCLS-II linac to the warm copper linac used by LCLS. In these figures the magnets are floating in space. Engineered support solutions will be developed in FY 2017.

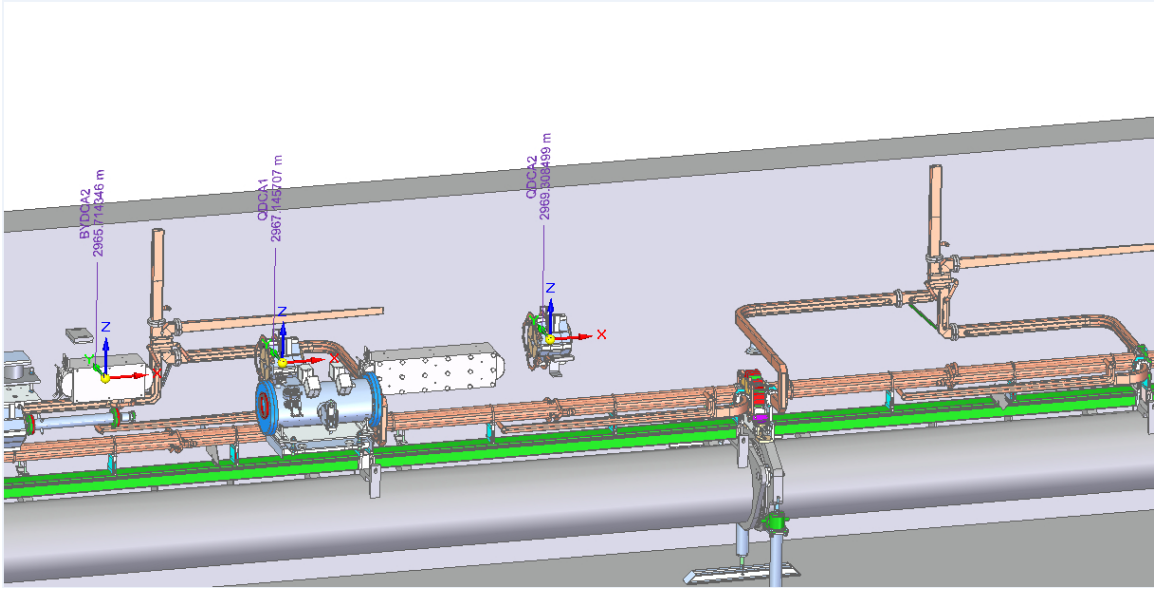

Figure 29: Isomorphic view of the beginning of the region where the DASEL beamline crosses over the warn copper linac.

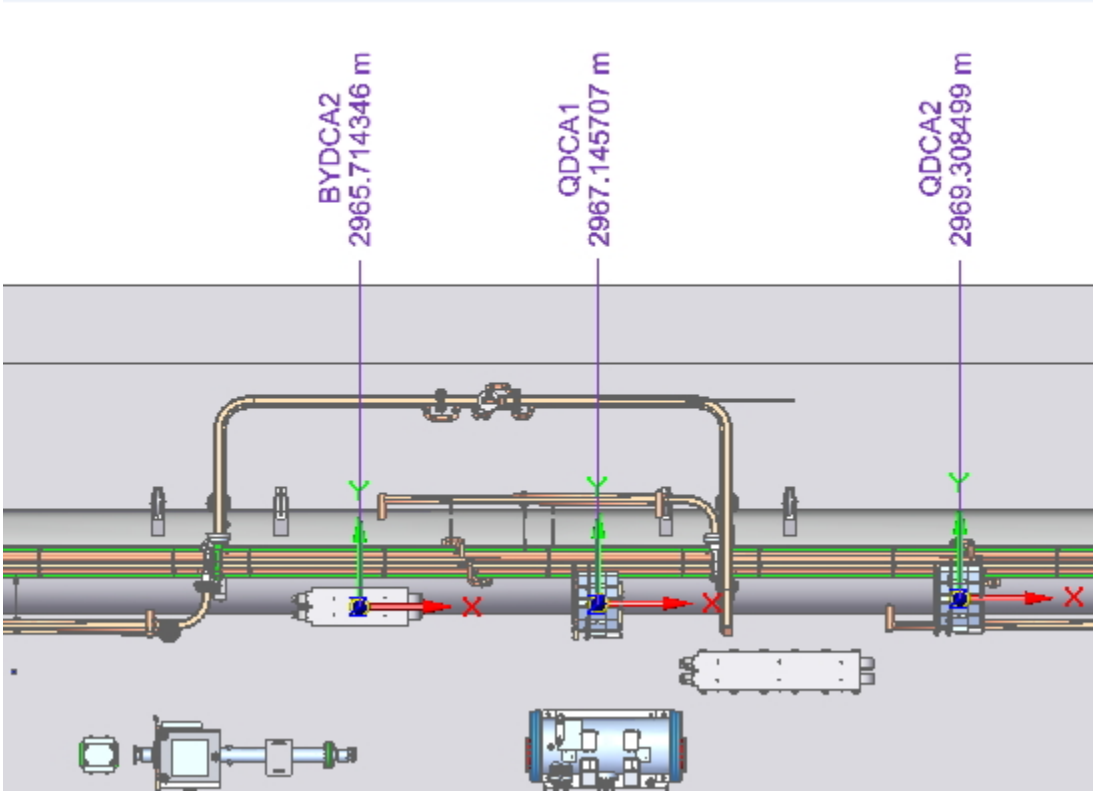

Figure 30. Plan view of the same part of the crossover region, indicating where magnets may need to be hung from the ceiling or from steel bands mounted to the large diameter copper linac support and alignment tube.

A full DASEL project proposal requires personnel to develop the kicker and source laser designs; the optical systems that integrate a kicker and septum to the LCLS-II beam and the magnetic elements to match the extracted beam and transport it to the experimental facility; and the design of the spoiler and collimation system. SLAC radiation safety personnel are required to set safety requirements and to review the BCS, PPS and MPS elements of the design.

Subsequent goals, for later in FY 2017 in the context of any required project review, include a detailed beamline design based when possible on pre-existing magnets, along with lists of vacuum, instrumentation, and power supply components. The engineering study needs an installation plan and appropriate project management milestones. Engineering specifications are needed for the kicker, the spoiler/collimation system and the source laser system, based on prototype studies, as required. At the end of the study, the cost estimate will be much more mature.

The project is currently managed by Tor Raubenheimer, Philip Schuster, and Natalia Toro. They coordinate the efforts by SLAC and external collaborators on the design of the experiments and oversee the interface to LCLS-II. They currently meet regularly with SLAC staff to assess progress and status. Throughout the process, they have consulted regularly with Joe Incandela of UCSB, John Jaros of SLAC; Jeremiah Mans of UOM, and Tim Nelson of SLAC regarding the experimental interface with the beamline.

4.2 DASEL Project Costs

4.2.1 Methodology

This is a bottoms-up cost estimate. Raw cost estimates were provided (see 4.2.2: Basis of Estimate) based on FY 2016 quotes and shop labor rates. Activities were divided into those occurring in FY 2018 and FY 2019. The raw costs were then escalated for inflation and SLAC overhead rates were applied. These rates applied are listed in

Table 3 below and were assumed constant for each fiscal year. For each item in the budget a design-maturity-based contingency was applied. Table 4 lists the range of contingency factors applied. Following standard practice, contingency is summed over items and held by management. The dollar value of the contingency and its percentage relative to the estimated cost (e.g., the escalated "raw cost" plus overhead) as a function of WBS category and cost type are presented in the cost summary tables that follow.

Table 3. Escalation, overhead, and contingency rates used in the cost estimate

Expense Type	Escalation	Overhead
Labor/Shop	3.50%	57.59%
M&S	2.50%	12.77%

Table 4. Design Maturity versus Contingency Applied

Design Maturity	M&S	Labor
Budgetary Quote	10%	10%
Engineered Design	15%	15%
Design Sketch	25%	25%
Design Concept	35%	35%
New Design Requiring R&D	35%	45%

4.2.2 Basis of Estimate

SLAC staff with knowledge of and access to LCLS-II cost data provided current, per-item FY 2016 cost estimates of M&S items. For example, each of the magnets, including the septum, is of a type of item that will be used by LCLS-II. LCLS-II plans to build three in-house “0.3625SD38.98” septa magnets and have the spare parts available to assemble a fourth one. It also has a detailed budget and production schedule. Likewise, LCLS-II plans to reuse many magnets from PEP-II and have allotted M&S and labor to refurbish them. The costs of the three “1.0D38.37” dipoles, two “1.0D22.625” dipoles and eleven “2Q4W” quadrupoles required by DASEL are projected based on LCLS-II experience.

By reusing DC magnets with archived field maps, we assume that only the septum and the kickers require detailed magnetic measurements and fiducialization. The vacuum components consist largely of commercial, off-the-shelf parts. Vacuum processing requirements are taken from recent LCLS-II experience.

The SLAC Power Conversion group used the field and current requirements for the 8 GeV beam to develop the detailed list of supplies, racks, and controllers. The same types of power supplies and racks are used by LCLS-II. As described earlier, the DASEL kicker is based on the same engineering concept as the LCLS-II kickers. The engineer building the LCLS-II kicker estimated the DASEL kicker cost.

The specialist in charge of installing similar beamlines to connect LCLS-II to the lines directed toward the undulators performed the labor estimate for the installation of the DASEL beamlines.

The SLAC Instrumentation and Controls Department tasked eight subject matter experts with estimating the labor and software costs associated with cabling, controlling and reading out the hardware seen by the beam (in turn, costed by mechanical and electrical engineers); they then estimated the hardware, labor, and software required by the radiation protection devices—Beam Containment System (BCS) and Personnel Protection System (PPS)—mandated by the SLAC Radiation Safety Group’s preliminary safety design.

The laser estimate was based on an informal quote for an amplifier and pulse picker from the company providing the 50W IR laser for LCLS-II. A significant cost savings is achieved by basing the design (Section 3.2) on reusing the rejected 46.4MHz pulses from the LCLS-II laser and transporting the IR light via fiber to the optical table near the RF gun and photocathode. The cost estimate for the LCLS-II laser UV conversion, pointing stabilization, laser controls, and diagnostics derives from the systems that LCLS-II has designed and budgeted for the same purposes.

For management, it was assumed that two physicists and an engineer at 50%, 25% and 25%, respectively, would be required each year to provide oversight and system integration. ES&H oversight during installation and Project Management & Cost Control oversight is provided for at the 10% FTE level.

4.2.3 DASEL Project Cost

This section redacted.

4.2.3.1 Cost Review

An independent cost and technical review was organized by the SLAC Deputy Director and the Associate Lab Directors of the Science and Accelerator Directorates on August 18-19, 2016. The reviewers identified several areas of possible cost reduction. Their recommendations were each acted upon in the following period and incorporated into the current document.

- The source laser was de-scoped from its original 186 MHz design to 46.4 MHz, thus allowing for the use of the LCLS-II laser. The bunch spacing is more suited to the first run of LDMX.
- Another family of PEP-II quadrupoles, “2Q4W”, was identified for use by DASEL. The original design called for the construction of 11 new “2Q10” quads with associated magnetic measurements.
- Several classes of “hidden contingency” were identified and removed. In some cases, prototype rather than production costs were used to estimate DASEL costs. In others, acknowledgement that LCLS-II concurrent work would facilitate and lower DASEL costs had not been made. Every effort has been made to present a best estimate for cost with management-controlled contingency allowing for changes to that estimate.

4.2.4 Schedule

The success of DASEL hinges on installing the beamline—but not necessarily the kicker and the laser—during the Oct. 2018-March 2019 period. All DC magnets other than the septum already exist on the SLAC site. The most time-critical magnet is the septum, which already has a detailed design and a 50 work-week LCLS-II production schedule. DASEL needs to begin construction of its septum as early in FY 2018 as possible and keep it consistent with LCLS-II planning.

“Resource loading” will be addressed in the next phase of the DASEL Design Study. We need to answer the questions of whether SLAC has the manpower to build and refurbish the extra devices and whether the installation labor exists within the lab at the same time as the installation team is busy with LCLS-II.

5 References

Please note that references 17-19 are internal LCLS-II project documents, but can be made available to interested parties.

1. R. Essig, P. Schuster, N. Toro and B. Wojtsekhowski, “An Electron Fixed Target Experiment to Search for a New Vector Boson A0 Decaying to e+e,” JHEP 1102, 009 (2011) [arXiv:1001.2557 [hep-ph]]; S. Abrahamyan *et al.* [APEX Collaboration], “Search for a New Gauge Boson in Electron-Nucleus Fixed-

Target Scattering by the APEX Experiment," Phys. Rev. Lett. 107, 191804 (2011) [arXiv:1108.2750 [hep-ex]].

2. https://confluence.slac.stanford.edu/display/hpsg/Project+Overview; M. Battaglieri, S. Boyarinov, S. Bueltmann, et al., "The Heavy Photon Search Test Detector," Nucl. Instrum. Meth. A 777 91 (2014), arXiv:1406.6115 [physics.ins-det].
3. J. Balewski et al., "DarkLight: A Search for Dark Forces at the Jefferson Laboratory Free-Electron Laser Facility," arXiv:1307.4432.
4. M. Battaglieri et al. [BDX Collaboration], "Dark matter search in a Beam-Dump eXper- iment (BDX) at Jefferson Lab," arXiv:1406.3028 [physics.ins-det].
5. H. Merkel et al. [A1 Collaboration] "Search for Light Gauge Bosons of the Dark Sector at the Mainz Microtron," Phys. Rev. Lett. 106, 251802 (2011); H. Merkel et al., "Search at the Mainz Microtron for Light Massive Gauge Bosons Relevant for the Muon g-2 Anomaly," Phys. Rev. Lett. 112 22, 221802 (2014) [arXiv:1404.5502 [hep-ex]]; M. Molitor, "Detectors for dark photon search with MESA," http://web.mit.edu/lns/PEB_Workshop/talks/Molitor_MESA_Study.pdf
6. M. Raggi and V. Kozhuharov, "Proposal to Search for a Dark Photon in Positron on Target Collisions at DAΦNE Linac," Adv. High Energy Phys, 2014, 959802 (2014) [arXiv:1403.3041 [physics.ins-det]].
7. S. Andreas et al., "Proposal for an Experiment to Search for Light Dark Matter at the SPS," arXiv:1312.3309 [hep-ex]; S. Gninenko "Search for dark sector physics in missing-energy events," https://p-348.web.cern.ch/sites/p-348.web.cern.ch/files/p348-gninenko-red.pdf
8. R. Essig, J. A. Jaros, W. Wester, et al., "Working Group Report: Dark Sectors and New, Light, Weakly-Coupled Particles" arXiv:1311.0029 [hep-ph].
9. "Dark Forces Below the Proton Mass Scale," APS April Meeting 2012; "New Forces at the GeV Scale and Dark Matter I-III," APS April Meeting 2015.
10. http://www.lnf.infn.it/conference/dark/
11. "Dark Interactions: Perspectives from Theory and Experiment," June 11-13, 2014 https://www.bnl.gov/di2014/ and October 4-7, 2016, https://www.bnl.gov/di2016/
12. "Light Dark Matter at Accelerators," June 24-26 2015 https://www.ge.infn.it/~ldma2015/LDMA2015/Welcome.html
13. J. Alexander et al., "Dark Sectors 2016 Workshop: Community Report", arXiv: 1608.08632 and http://www-conf.slac.stanford.edu/darksectors2016/
14. E. Izaguirre, G. Krnjaic, P. Schuster and N. Toro, "Testing GeV-Scale Dark Matter with Fixed-Target Missing Momentum Experiments, PRD91 (2015) 9, 094026, arXiv:1411.1404 [hep-ph].
15. E. Izaguirre, G. Krnjaic, P. Schuster, N. Toro "Analyzing the Discovery Potential for Light Dark Matter," PRL 115 (2015) 25, 251301, arXiv:1505.00011 [hep-ph].
16. https://indico.fnal.gov/contributionDisplay.py?contribId=422&confId=6890; https://indico.fnal.gov/contributionDisplay.py?contribId=423&confId=6890;

https://confluence.slac.stanford.edu/download/attachments/192193555/SuperHPS_NEXT.pdf?version=1&modificationDate=1452628699000&api=v2

17. See Table 1 of "LCLS-II Timing System Physics Requirements Document," LCLSII-2.7-PR-0345 (2015).
18. "LCLS-LL SCRF Injector System Physics Requirements Document," LCLSII-2.2-PR-0084 (2014).
19. "LCLS-II Spreader Kicker Engineering Specifications Document," LCLSII-2.4-ES-0494 (2015).